UNCLASSIFIED

AD NUMBER
AD859276
LIMITATION CHANGES

TO:

Approved for public release; distribution is unlimited.

FROM:

Distribution authorized to U.S. Gov't. agencies and their contractors; Administrative/Operational Use; MAY 1969. Other requests shall be referred to Army Aviation Labs., Fort Eustis, VA.

AUTHORITY

USAAMRDL ltr 18 Jun 1971

THIS PAGE IS UNCLASSIFIED

AD859276

AD

USAAVLABS TECHNICAL REPORT 68-49D

AN INVESTIGATION OF THE DYNAMIC STABILITY CHARACTERISTICS OF A QUAD CONFIGURATION, DUCTED-PROPELLER V/STOL MODEL

VOLUME IV

THE LONGITUDINAL STABILITY CHARACTERISTICS OF A QUAD CONFIGURATION, DUCTED-PROPELLER V/STOL MODEL AT HIGH DUCT INCIDENCE

By

Howard C. Curtiss, Jr.

May 1969

U. S. ARMY AVIATION MATERIEL LABORATORIES
FORT EUSTIS, VIRGINIA
CONTRACT DAAJ02-67-C-0025
DEPARTMENT OF AEROSPACE AND MECHANICAL SCIENCES
PRINCETON UNIVERSITY
PRINCETON, NEW JERSEY

98

DEPARTMENT OF THE ARMY
HEADQUARTERS US ARMY AVIATION MATERIEL LABORATORIES
FORT EUSTIS, VIRGINIA 23604

This report has been reviewed by the U. S. Army Aviation Materiel
Laboratories, the Naval Air Systems Command, and the Air Force
Flight Dynamics Laboratory. It is considered to be technically
sound.

The data from a series of experiments conducted to measure the
longitudinal transient response characteristics of a dynamically
similar quad-duct V/STOL aircraft similar to the X-22A configura-
tion are analyzed to determine the stability derivatives of the
vehicle at five duct incidences. The Princeton Dynamic Model
Track was utilized to perform the series of experiments.

This report is published for the exchange of information and the
stimulation of ideas.

AN INVESTIGATION OF THE DYNAMIC STABILITY
CHARACTERISTICS OF A QUAD CONFIGURATION,
DUCTED-PROPELLER V/STOL MODEL

Volume IV.

**THE LONGITUDINAL STABILITY CHARACTERISTICS OF A
QUAD CONFIGURATION, DUCTED-PROPELLER V/STOL MODEL
AT HIGH DUCT INCIDENCE.**

Aerospace Sciences Report 848

By

Howard C. Curtiss, Jr.

Prepared by

Department of Aerospace and Mechanical Sciences
Princeton University
Princeton, New Jersey

for

U. S. ARMY AVIATION MATERIEL LABORATORIES
FORT EUSTIS, VIRGINIA

SUMMARY

The results of experiments conducted to determine the dynamic stability characteristics of a dynamically similar model of a quad-duct V/STOL aircraft are reported in References 1 and 2. Portions of these data that pertain to the longitudinal dynamics of the vehicle at five duct incidences were analyzed to determine the stability derivatives of the vehicle. The analysis and the resulting stability derivatives are presented and discussed in this report.

The measured time histories indicated that the data could be analyzed on the basis of linearized small perturbation equations. Root locus techniques were used to analyze the data.

The full-scale derivatives determined from the analysis that correspond to a vehicle very similar to the Bell X-22A are presented.

The transient motions of the model were unstable at all duct incidences except 50°, the lowest incidence investigated.

TABLE OF CONTENTS

LIST OF ILLUSTRATIONS

LIST OF TABLES

LIST OF SYMBOLS

b	propeller blade chord, feet
C_m	mechanical damping, due to friction, foot-pounds/radian/second
c	duct chord, feet
cg	center of gravity of pivoting mass of model
d	propeller blade diameter, feet
FS	fuselage station (horizontal reference), inches
g	acceleration due to gravity, feet per second squared
h	altitude, feet
I_y	model moment of inertia in pitch about pivot axis, slug-feet squared
i	$\sqrt{-1}$
i_d	duct incidence, degrees
$K_{\dot{\theta}}$	feedback gain, proportionality constant between differential blade angle change and angular velocity in pitch, seconds
k_y	radius of gyration, feet
k_{θ_m}	mechanical spring constant, foot-pounds per radian
$M_u, M_w,$ $M_{\dot{w}}, M_{\dot{\theta}}$	stability derivatives, rate of change of pitching moment divided by inertia I_y with variable indicated in subscript
$M_{\Delta\beta_{PITCH}}$	longitudinal control effectiveness, rate of change of pitching moment divided by inertia I_y with propeller differential collective pitch, per second squared
$\bar{M}_{\dot{\theta}}$	augmented pitch damping stability derivative $(\bar{M}_{\dot{\theta}} = M_{\dot{\theta}} + K_{\dot{\theta}} M_{\Delta\beta_{PITCH}})$, per second

m	mass accelerated by the model when translating vertically, slugs ($m = m_p + m_v = 1.60$ slugs)
m_h	mass of horizontal travel link, slugs ($m_h = 0.11$ slug)
m_p	pivoting mass of model, slugs ($m_p = 1.48$ slugs)
m_t	total mass accelerated by the model when translating horizontally, slugs ($m_t = m + m_h + 1.71$ slugs)
$\dfrac{m}{m_t}$	ratio of vertical to horizontal masses ($\dfrac{m}{m_t} = 0.936$)
m_v	mass of vertical travel link, slugs ($m_v = 0.12$ slug)
R	propeller blade radius, feet
r	distance along propeller radius (measured from axis of rotation), feet
$\dfrac{r}{R}$	propeller blade radial station
rpm	model propeller rotational speed, revolutions per minute
s	Laplace operator, or root of characteristic equation, per second ($s = \sigma + i\omega$)
t	propeller blade thickness, feet
U	aircraft velocity along body-fixed X axis (stability axis system), feet per second ($U = U_o + u$)
U_f	aircraft horizontal velocity (space-fixed axis system), feet per second ($U_f = U_{o_f} + u_f$)
U_o	aircraft initial velocity along flight path (stability axis system) feet per second
U_{o_f}	aircraft initial horizontal velocity (space-fixed axis system), feet per second
u	aircraft perturbation velocity along body-fixed longitudinal axis (stability axis system), feet per second
u_f	aircraft horizontal perturbation velocity (space-fixed axis system), feet per second

V	flight velocity, feet per second
W_f	aircraft vertical velocity (space-fixed axis system), feet per second ($W_f = W_{o_f} + w_f$)
W_{o_f}	aircraft initial vertical velocity (space-fixed axis system), feet per second
W_p	model pivoting weight, pounds ($W_p = 47.5$ pounds)
w	aircraft perturbation velocity along body-fixed Z axis (stability axis system), feet per second
w_f	aircraft vertical perturbation velocity (space-fixed axis system), feet per second
WL	fuselage water line (vertical reference station), inches
X	body-fixed longitudinal axis, initially aligned into the relative wind (stability axis system)
X_f	horizontal axis (space-fixed axis system)
X'	perturbed location of X_f
X_u, X_w, X_θ	stability derivatives, rate of change of longitudinal force divided by the mass m with variable indicated in subscript
x_{cg}	longitudinal distance of cg from pivot axis, inches
x_{pivot}	longitudinal position of model pivot axis referenced to FS 0, inches (model scale unless noted)
$\bar{x}$	axial distance (coordinate) from duct leading edge, inches (full scale)
Y_f	lateral axis (space-fixed axis system)
Y'	perturbed location of Y_f
$\bar{y}$	radial distance (coordinate) from duct center line, inches (full scale)
Z	body-fixed vertical axis, initially aligned perpendicular to the relative wind in the vertical plane (stability axis system)

Z_f vertical axis (space-fixed axis system), aligned with g

$Z_u, Z_w,$ stability derivatives, rate of change of vertical force divided
$Z_{\dot{\theta}}$ by mass m with variable indicated in subscript

Z' perturbed location of Z_f

z_{cg} vertical distance of cg from pivot axis, inches

z_{PIVOT} vertical position of model pivot axis referenced to WL 0,
inches (model scale unless noted)

β local propeller blade angle, degrees

β_f average propeller blade angle on the two front propellers,
degrees

β_R average propeller blade angle on the two rear propellers,
degrees

$\beta_{.75R}$ average propeller blade angle required for vertical force trim
(collective pitch) measured at the three-quarter radius and
averaged for four propellers, degrees

$\Delta M_{\dot{u}_{cg}}$ additional stability derivative due to vertical displacement
of cg from pivot axis, per foot $\left(\Delta M_{\dot{u}_{cg}} = -\dfrac{m_p\, z_{cg}}{I_y}\right)$

$\Delta M_{\dot{u}_{ps}}$ additional stability derivative due to control system,
per foot ($i_d = 60°$ only)

$\Delta M_{\dot{w}_{cg}}$ additional stability derivative due to horizontal displacement
of cg from pivot axis, per foot $\left(\Delta M_{\dot{w}_{cg}} = \dfrac{m_p\, x_{cg}}{I_y}\right)$

$\Delta M_{\theta_{cg}}$ additional stability derivative due to vertical displacement
of cg from pivot axis, per second squared $\left(\Delta M_{\theta_{cg}} = -\dfrac{W_p\, z_{cg}}{I_y}\right)$

ΔM_{θ_m} additional stability derivative due to mechanical spring,
per second squared $\left(\Delta M_{\theta_m} = -\dfrac{k_{\theta_m}}{I_y}\right)$

$\Delta M_{\dot{\theta}}$ increment in pitch damping due to feedback, per second $\left(\Delta M_{\dot{\theta}} = K_{\dot{\theta}} \, M_{\Delta \beta_{PITCH}} \right)$

$\Delta \beta$ change in propeller blade angle, degrees (positive for trailing edge down with duct at 90° incidence)

$\Delta \beta_O$ longitudinal control required for pitching moment trim (differential collective pitch), degrees or radians $\left(\Delta \beta_O = \dfrac{\beta_R - \beta_F}{2} \right)$

$\Delta \beta_{PITCH}$ longitudinal control input due to stability augmentation, degrees $\left(\Delta \beta_{PITCH} = \dfrac{\Delta \beta_{RS} + \Delta \beta_{RP}}{4} - \dfrac{\Delta \beta_{FS} + \Delta \beta_{FP}}{4} \right)$

$\Delta_{\theta,u}$ characteristic equation for two-degree-of-freedom motion in θ-U_f

$\left(\Delta_{\theta,u} \right)_O$ characteristic equation for two-degree-of-freedom motion in θ-U_f with $M_w = 0$

δ elevon deflection, degrees (positive for trailing edge forward with duct at 90° incidence)

θ fuselage pitch angle, degrees or radians (positive nose up)

Λ_L gross weight scale factor $= \dfrac{\text{desired gross weight}}{\text{gross weight determined on basis of dynamic scaling}}$

λ_L linear scale factor $\lambda_L = \dfrac{\text{model length}}{\text{full-scale length}}$

ρ ambient mass density of air, slugs per cubic foot

σ real part of characteristic root, per second

Ω propeller rotational speed, rpm or radians per second

ω frequency, imaginary part of characteristic root, per second

ω_N undamped natural frequency, per second

$(\dot{\ })$ differentiation with respect to time

$(\ )_c$ full-scale parameter determined by dynamic scaling laws

$(\ )_0$ full-scale parameter at selected gross weight

$(\ )_{f_p}$ control deflection associated with front port duct

$(\ )_{f_s}$ control deflection associated with front starboard duct

$(\ )_{r_p}$ control deflection associated with rear port duct

$(\ )_{r_s}$ control deflection associated with rear starboard duct

INTRODUCTION

References 1 and 2 present data from a series of experiments conducted to measure the longitudinal transient response characteristics of a dynamically similar quad-duct V/STOL model using the Princeton Dynamic Model Track. This program is part of a continuing effort using the Princeton Dynamic Model Track to provide data on the dynamic stability of V/STOL aircraft at low speeds. The model is similar in configuration to the Bell X-22A, with a scale factor of 0.145. The model is shown mounted on the test apparatus in Figure 1. A close-up view of the model is shown in Figure 2. A general arrangement drawing of the model is given in Figure 3. Differences between the Bell X-22A and this research model are described in the section entitled Description of Apparatus and Experiments.

This report analyzes the data from References 1 and 2 to determine the longitudinal stability derivatives of the vehicle in low-speed/high-duct-incidence flight conditions, including hovering flight. The test program is described in detail in References 1 and 2; thus, only a brief discussion of the program is included in this report. The test conditions analyzed are listed in Table I.

Transient measurements in the flight conditions of interest indicated that the dynamic motions of the model could be described by conventional, linearized small-perturbation equations. The following analysis is based on that assumption. Discussion of the analysis of the data is phrased in terms of model parameters. The values of the stability derivatives of the full-scale aircraft are discussed in the section entitled Stability Derivatives of the Full-Scale Aircraft. The scaling laws used to design the model result in the conversion factors given in Table II, which are used for interpretation of model data in full-scale terms.

The model was found to be dynamically unstable at all but the lowest duct incidence examined. Data were taken on the response of the basic model, as well as with varying amounts of rate feedback (fore and aft differential propeller blade angle proportional to pitching rate), to assist in the analysis.

It will be noted that in the flight conditions at duct incidences of $60°$ and $50°$, the cg of the model was displaced from the pivot axis of the model. Balance weights were added to the model at these trim conditions to reduce the amount of differential propeller blade angle required for pitching moment equilibrium.

For analysis purposes, it is possible to locate the origin of the axis system either at the cg of the model or at the pivot axis. It was considered to be more convenient to locate the origin of the axis system at the pivot axis and to add terms to account for the displacement of the cg from this location. The stability derivatives are presented about the

1

pivot axis, which corresponds to the cg position of the Bell X-22A given in Reference 3 (WL 139, FS 312). All linear velocities of the model are the linear velocities of the pivot axis.

Various methods of analyzing the data are possible. A convenient approach, when limited-degree-of-freedom data are available, employs root locus techniques as described in the section entitled Experimental Results and Analysis of Data.

While only the frequency and damping characteristics of the motions are presented and used in the analysis, various other properties of the time histories may be used to provide additional information. Other measured data, such as the phase angle between the pitch angle and the horizontal velocity perturbation, were used to check the results obtained from the method of analysis described in the text that follows.

DESCRIPTION OF APPARATUS AND EXPERIMENTS

TEST FACILITY

The Princeton Dynamic Model Track is designed expressly for the study of the dynamic motions of helicopter and V/STOL models at equivalent flight speeds of up to 60 knots (for a one-tenth scale model). Basic components of the facility include a servo-driven carriage riding on a track 750 feet long, located in a building with a cross section of 30 by 30 feet; the carriage has an acceleration potential of 0.6g and a maximum speed of 40 feet per second. A detailed description of the facility and the testing techniques employed may be found in Reference 4.

A model can be attached to the carriage by one of several booms. The mount used to conduct longitudinal investigations is shown in Figure 1. This mount permits relative displacements of the model with respect to the carriage in horizontal and vertical directions. The model is supported on a three-axis gimbal system that allows selection of any or all of the three angular degrees of freedom. Horizontal relative motion of the model with respect to the carriage is sensed and used to command the carriage to follow the model in a closed-loop fashion. Similarly, vertical displacement of the model with respect to the carriage commands the boom to move vertically. This servo operation of the carriage allows the model to fly "free", with no restraints on the dynamic motions being investigated. This method of testing may be considered to be similar to dynamic flight testing, but considerably more control over the experiment is possible.

MODEL

A photograph of the model is shown in Figure 2. A general arrangement drawing is presented in Figure 3. Figure 4 shows the pivot axis, cg location, and reference locations of the model. The model's pertinent dimensions and inertia characteristics are listed in Table III. The model was designed as a general research model for investigation of the dynamic stability characteristics of various quad configuration V/STOL aircraft as described in Reference 5.

This dynamic model is powered by a 200-volt, 400-cycle, 3-phase electric motor. The motor drives the four ducted propellers through a central transmission and various right-angle gearboxes. The aerodynamic shape of the model is obtained through the use of a Fiberglas skin with Styrofoam stiffeners. The propeller blades are made with a plastic foam core and Fiberglas skin. The geometric characteristics of the propeller are shown in Figure 5, and the geometric characteristics of the duct and elevon are shown in Figures 6 and 7. The duct shape is identical to that of the Bell X-22A aircraft.

3

Model control positions are set from a control console on the carriage.
The blade pitch angles of each of the four propellers are electrically
controllable. Also, the deflection angles of the elevons are electrically
controllable. All of these control systems are closed-loop position
controls and are used as such in the portions of the experiments involving
feedback to alter the transient motions of the model. The dynamic charac-
teristics of these feedback loops are such that the time response of the
control is negligible in the frequency range of interest. Although the
control servo loops are nonlinear, using polarized relays for power ampli-
fication, they can be characterized as having a closed-loop natural
frequency of approximately 10 cycles per second, with a damping ratio of
approximately seven-tenths. The servo gear ratios were selected so that
the rate limits arising from the rpm limitations of the control drive
motors were equal to, or greater than, scaled rate limits determined from
full-scale Bell X-22A values, as given in Reference 3.

This research model differs from the Bell X-22A in the following
particulars:

1. The elevon on the model differs from that on the full-scale air-
   craft. The model elevon has no movable surface forward of the
   hinge line, and its hinge line is located below the trailing edge
   of the duct, as shown in Figure 7. While these differences would
   affect the control effectiveness and the control loads, they,
   would not be expected to have any significant effect on the
   dynamic motions.

2. The duct rotation point is at a different location on the model
   (84 percent c) than on the full-scale aircraft (55 percent c).

   With the ducts at 90° incidence, the propeller hubs are in the
   same relative position on the model as they are on the full-scale
   aircraft. The cg of the model is higher (1.2 percent c) on the
   model, with respect to the propeller hubs, than it is on the
   full-scale aircraft.

3. For the tests at 90°, 80°, and 70° incidence, the vertical tail
   on the model is smaller than the one on the full-scale vehicle,
   as shown in Figure 3. The scaled vertical tail, also shown in
   Figure 3, was used for the tests at duct incidences of 60° and
   50°. This difference in vertical tail area would not have a
   significant effect on the longitudinal dynamic stability charac-
   teristics.

This model was planned as a general research model; numerous other quad
configuration layouts can be simulated through the use of interchangeable
parts as described in Reference 5. No attempt was made in the design
stage to simulate the X-22A precisely. However, the modifications de-
scribed above will not result in appreciable differences in the model
dynamic stability characteristics.

4

EXPERIMENTS

The experiments that were conducted to determine the stability character-
istics of the model consisted of transient response measurements in
various longitudinal degrees of freedom. The data are presented in
References 1 and 2, and the test conditions are given in Table I. Measure-
ments were also made with various levels of rate feedback. Since the
model was unstable, or at best neutrally stable, in the majority of flight
conditions investigated, no predetermined control inputs were used to
excite the motion of the model.

EXPERIMENTAL RESULTS AND ANALYSIS OF DATA

The transient response data presented in References 1 and 2 were analyzed to determine the period and damping of the longitudinal modes of motion of the model at five duct incidences: 90°, 80°, 70°, 60°, and 50°. The trim condition was level flight, and the fuselage attitude was set equal to zero in trim. Experimentally determined model trim conditions are shown in Figure 8. The data and the results of the analysis are discussed in terms of model parameters in this section. A detailed numerical example of the analysis procedure at a duct incidence of 70° is presented in Appendix II.

First, it is desirable to make a few remarks regarding the analysis of transient response data for higher than second-order systems. If a system has an unstable mode present in its transient response, it is difficult to measure (from the time history of the motion) the characteristics of any mode but the unstable one, which will dominate the motion irrespective of the nature of the disturbance. Therefore, certain practical limitations are placed on the determination of all of the stability derivatives of an unstable aircraft, since the characteristics of all the modes cannot be accurately determined. This limitation in analyzing transient response data of multiple-degree-of-freedom systems can be surmounted by the use of limited-degree-of-freedom tests, as may be seen from the following discussion.

The measured characteristics of the transient response consist of the frequency and damping characteristics of the dominant unstable mode. When a component of the transient motion is purely divergent, it has been found difficult to measure the value of the positive real root corresponding to the divergence. Therefore, transient response data which involve a divergent mode have not been analyzed quantitatively. Divergent motions were eliminated in the single-degree-of-freedom tests (θ only) through the use of a mechanical spring. The test conditions in which a pure divergence was present were two-degree-of-freedom motions (θ-w_f) at duct incidences 80°, 70°, and 60°.

Four different combinations of degrees of freedom were measured at all of the duct incidences except hover: one single-degree-of-freedom motion, θ, ($U_f = 0$, and $w_f = 0$); two two-degree-of-freedom motions, θ-w_f, ($U_f = 0$), and θ-U_f, ($w_f = 0$); and the complete longitudinal three-degree-of-freedom motion (θ-U_f-w_f). The development of the equations of motion that are assumed to apply to the data is presented in Appendix I. Note that the following discussion is phrased in terms of space-fixed degrees of freedom in accordance with the manner in which the tests were conducted. The space-fixed axis system is shown in Figure 9, and the transformation from a stability axis system to a space-fixed axis system is discussed in Appendix I.

6

Measured transient characteristics are presented at the various duct inci-
dences on the complex plane in Figure 10. Frequency and damping charac-
teristics of the dominant mode are presented as a function of rate feed-
back gain and degrees of freedom of the test. The characteristic roots of
the single-degree-of-freedom motion are presented as calculated with the
mechanical spring removed (see Appendix II).

The following general approach was used to determine the stability deriva-
tives. To simplify the discussion, known additional terms due to the
displacement of the cg of the model from the pivot axis and due to the
model mounting linkage mass are not included in the discussion that
follows (see Appendix I).

ONE DEGREE OF FREEDOM

First, the one-degree-of-freedom results were analyzed. At all duct inci-
dences except $i_d = 50°$, a mechanical spring was added about the pitch axis
of the model to provide a restoring moment proportional to model attitude
such that the angular motion of the model would be oscillatory, and thus
could be analyzed more accurately in the flight conditions where the
angle-of-attack stability of the model was positive $(M_w U_{o_f} > 0)$. Positive

angle-of-attack stability will result in a divergent motion of the model
in one degree of freedom if no restoring spring is provided. The spring
constant of the mechanical spring was selected so that the frequency of
motion in one degree of freedom was similar to the frequency of the free
motion of the model in the multiple-degree-of-freedom tests. At the
highest speed (lowest duct incidence) tested, the angle-of-attack stability
was negative $(M_w U_{o_f} < 0)$ and therefore no spring was used.

As shown in Appendix I, the equation of motion that applies to the single-
degree-of-freedom tests is equation (18), with $z_{cg} = 0$.

$$\ddot{\theta} - \left(M_{\dot{\theta}} + M_{\dot{w}} U_{o_f} \right) \dot{\theta} + \left(\frac{k_{\theta_m}}{I_y} - M_w U_{o_f} \right) \theta = 0 \qquad (1)$$

k_{θ_m} is the spring constant of the mechanical spring and is determined by
calibration prior to the experiment. The two terms in equation (1), the
coefficients of $\dot{\theta}$ and θ, are determined by the frequency (ω_N) and damping
(σ) measured from the transient response data (listed in Table I). De-
rivatives, or combinations of derivatives, are found from the relation-
ships

7

$$- M_w U_{o_f} = \omega_N^2 - \frac{k_{\theta_m}}{I_y}$$

$$+ M_{\dot\theta} + M_{\dot w} U_{o_f} = 2\sigma \qquad (2)$$

Values of the derivatives calculated from the measured characteristics of
the transients and the expressions of equation (2) are listed in Table IV.

TWO DEGREES OF FREEDOM

The stability derivatives obtained from the single-degree-of-freedom runs
are now used in conjunction with the data from the two-degree-of-freedom
experiments involving pitch angle and horizontal velocity to find other
stability derivatives. The equations which describe the motion in this
case are equations (16), given in Appendix I, with m/m_t equal to one and
z_{cg} equal to zero.

$$\dot u_f - X_u u_f + (g - X_w U_{o_f})\, \theta = 0$$

$$- M_u u_f + \ddot\theta - (M_{\dot\theta} + M_{\dot w} U_{o_f})\, \dot\theta - M_w U_{o_f}\, \theta = 0 \qquad (3)$$

While three characteristic roots are necessary to delineate this dynamic
condition, only the two which determine the oscillatory mode character-
istics can be evaluated, as discussed previously. There are three
additional derivatives present in equations (3): $X_u, M_u,$ and X_w. As may
be seen from the discussion that follows, it is possible to calculate only
the term X_w in combination with M_u. Analysis of isolated duct data indi-
cates that the term $X_w U_{o_f}$ is negligible compared to g.

A convenient way of calculating the two unknown derivatives X_u and M_u is
to place equations (3) in root locus form, considering M_u as a variable
quantity. The Laplace transform of equations (3) is taken, and the charac-
teristic equation is calculated; then, the characteristic equation is
arranged in root locus form as

$$\frac{M_u\,(g - X_w U_{o_f})}{(s - X_u)(s^2 - [M_{\dot\theta} + M_{\dot w} U_{o_f}]\, s - M_w U_{o_f})} = -1 \qquad (4)$$

Now, the characteristic roots of the quadratic factor in the denominator
of equation (4) have been determined from the single-degree-of-freedom

8

tests [equation (1)] and are shown in Figure 11 ($\triangle$). The derivative X_u is then specified by the condition that the root locus for variable M_u must pass through the experimentally measured data ($\odot$), as shown in Figure 11.

The stability derivative M_u is determined from the gain $[M_u (g - X_w U_{o_f})]$ required for the calculated roots to agree with the experimentally measured roots. The derivative values that were found are listed in Table IV.

Since the two-degree-of-freedom experiments were conducted with various levels of rate feedback, a verification of the calculated value of X_u is possible. It is assumed that fore and aft differential propeller blade angle produces only a pitching moment, and that there is no lag between the rate signal ($\dot{\theta}$) and the control actuation ($\Delta\beta_{PITCH}$), so that the effect of rate feedback may be included as an increment in pitch damping, $\Delta M_{\dot{\theta}}$.

The increment produced by the rate feedback is also calculated. The characteristic equation derived from equations (3) is rearranged in a form expressing $\Delta M_{\dot{\theta}}$ as variable.

$$\frac{- \Delta M_{\dot{\theta}} (s - X_u) s}{[s - X_u][s^2 - (M_{\dot{\theta}} + M_{\dot{w}} U_{o_f}) s - M_w U_{o_f}] + M_u (g - X_w U_{o_f})} = -1 \qquad (5)$$

The roots of the polynomial in the denominator of this expression, i.e., the poles for the root locus, are the characteristic dynamics with no feedback. These are known from the two-degree-of-freedom analysis with no feedback. The zero for the root locus based on equation (5) is located on the real axis at X_u. Therefore, the value of X_u is verified from the condition that this locus, drawn for $\Delta M_{\dot{\theta}}$ varying, corresponding to various feedback gains, intersects the experimentally determined dynamics for various feedback gains.

The increments in pitch damping, as a function of rate feedback gain, determined by this procedure, are given in Table IV. The value of X_u determined by this approach agreed closely at all duct incidences with the value determined from the unstabilized model responses.

Two-degree-of-freedom motions, consisting of pitching and vertical velocity, were also measured. At all incidences except 50°, the character of this motion was divergent; thus, no analysis was attempted because of the difficulty, previously mentioned, of making quantitative measurements of divergent motions. At 50° incidence, the characteristics of this two-

9

degree-of-freedom motion may be used to determine Z_w, as seen from equation (17) in Appendix I, with x_{cg} and z_{cg} equal to zero, as follows:

$$\dot{w}_f - Z_w w_f - Z_w U_{o_f} \theta = 0$$

$$- M_{\dot{w}} \dot{w}_f - M_w w_f + \ddot{\theta} - (M_{\dot{\theta}} + M_{\dot{w}} U_{o_f}) \dot{\theta} - M_w U_{o_f} \theta = 0 \qquad (6)$$

Comparison of equations (6) with the single-degree-of-freedom case [equation (1)] shows that there is one additional stability derivative present in equations (6); that derivative is Z_w. The downwash lag derivative ($M_{\dot{w}}$) now appears separately from the pitch damping derivative ($M_{\dot{\theta}}$); it is therefore possible to obtain an indication of the size of this derivative from a root locus drawn with Z_w as a variable parameter. The root locus equation developed from equations (6) takes the following form:

$$\frac{- Z_w (s - M_{\dot{\theta}}) s}{s(s^2 - [M_{\dot{\theta}} + M_{\dot{w}} U_{o_f}]s - M_w U_{o_f})} = - 1 \qquad (7)$$

The locations of the two poles, determined from the quadratic factor in the denominator of equation (7), are the single-degree-of-freedom roots, equation (1), and therefore are known. The pitch damping is determined from the condition that the locus of roots with variable Z_w intersects the experimental points. The value of Z_w is calculated from the gain required for coincidence of the calculated and measured roots. At the one duct incidence, $50°$, where this analysis was made, indications were that $M_w U_{o_f}$ was negligible compared to $M_{\dot{\theta}}$.

THREE DEGREES OF FREEDOM

The three-degree-of-freedom motions were analyzed, and the derivatives Z_u and Z_w were calculated. In most cases, in the low-speed flight regime, these derivatives are quite small, producing only small changes between the two-degree-of-freedom ($\theta-U_f$) motion and the three-degree-of-freedom ($\theta-U_f-w_f$) motion (Figure 10).

If X_w and $M_{\dot{w}}$ are assumed to be negligible, then the three-degree-of-freedom characteristic equation developed from equations (15), in Appendix I, may be expressed in the following form:

$$s \; \Delta_{\theta,u} - Z_w \left[(\Delta_{\theta,u})_0 - M_w \frac{Z_u \delta}{Z_w} \right] = 0 \qquad (8)$$

where $\Delta_{\theta,u}$ is the characteristic equation of the two-degree-of-freedom motion and $(\Delta_{\theta,u})_0$ is the characteristic equation of the two-degree-of-freedom motion with $M_w = 0$. From equation (8) it may be noted that if M_w is equal to zero, or if Z_u and Z_w are zero, then there is no difference between characteristic dynamics of the two-degree-of-freedom motion involving θ and U_f and the three-degree-of-freedom motion $(\theta-U_f-w_f)$ aside from the extra root. It is assumed that X_w is negligible, and this is used for the duct incidences in which there are measurable differences between the two- and three-degree-of-freedom motions. The polynomials $\Delta_{\theta,u}$ and $(\Delta_{\theta,u})_0$ have known coefficients from the two-degree-of-freedom analysis. Equation (8) is rearranged in root locus form as

$$\frac{- Z_w \left[(\Delta_{\theta,u})_0 - M_w \frac{Z_u \delta}{Z_w} \right]}{s \; \Delta_{\theta,u}} = -1 \qquad (9)$$

Now the value of the quantity $Z_u g/Z_w$ will determine the location of the zeros of equation (9). It is found that the locus of roots for Z_w varying, at a constant value of the ratio Z_u/Z_w, must intersect the experimentally measured values of the frequency and damping. The value of Z_w is calculated from the gain required for coincidence of the calculated and experimental points. Then, Z_u is determined from the known $Z_u g/Z_w$. The stability derivatives determined in this fashion are listed in Table IV.

This procedure was generally followed at all duct incidences, to evaluate the stability derivatives of the vehicle, with minor variations as noted below.

$i_d = 90^\circ$

Only the single- and two-degree-of-freedom $(\theta-u_f)$ motions were analyzed. Experimental results showed, as would be expected from symmetry considerations, that the w_f motion was not coupled to the $(\theta-u_f)$ motion. It is not possible to determine Z_w in hovering because of the nature of the tests conducted.

In hover, three test conditions representing different blade angle and

11

propeller rpm settings were investigated. Two of the test conditions utilize different combinations of blade angle and rpm to produce the same total thrust (vertical force equal to the weight of the model): $\beta_{.75R}$ equal to 25.8 degrees, rpm equal to 7000; and $\beta_{.75R}$ equal to 29.2 degrees, rpm equal to 6400. The third test condition uses another combination of blade angle and rpm, resulting in a lower total thrust than previous cases: $\beta_{.75R}$ equal to 25.8 degrees, rpm equal to 6400. This combination of blade angle and rpm produces a hover thrust of 43.1 pounds, corresponding to a scaled gross weight of 14,000 pounds for the Bell X-22A. Note that the weight of the model is 51.5 pounds in all cases, so that only two-degree-of-freedom (θ-u_f) motions were examined in the low thrust case.

Dimensional analysis can be used to demonstrate that for the two test conditions at the same propeller blade angle, if the time scale of the dynamics is nondimensionalized by the rpm, then the nondimensional frequency and damping should be independent of the rpm. This comparison of the two test cases is shown in Figure 10. The spread in the points is considered to be within the accuracy with which frequency and damping can be evaluated from the highly unstable dynamics of this hovering motion.

If the dynamic stability of the vehicle depends only on the geometric configuration of the vehicle and the duct exit velocity, then there should be no difference between the dynamic characteristics at the same total thrust level produced by different combinations of blade angle and rpm. There are measurable differences, although not large, between these two test conditions. The results indicate that it is desirable to conduct dynamic stability tests at the proper blade angle.

$i_d = 80°$

The procedure described above for $i_d = 90°$ was followed. No measurable difference existed between the two-degree-of-freedom motion (θ-U_f) and the three-degree-of-freedom motion (θ-U_f-w_f); thus, Z_w and Z_u were not determined. That is, similar to the hovering case, there is only weak coupling between the (θ-U_f) degrees of freedom and the w_f degree of freedom. It is expected that Z_w has a value in this flight condition as it has in hover, but it cannot be determined from the experiments conducted.

$i_d = 70°$

The analysis at this trim condition is discussed in detail in Appendix II, and the transient response data are shown in Figures 17 through 28. The transient response of the model in two degrees of freedom (θ-U_f), shown in Figure 18, exhibited a rate of growth of the dominant unstable oscillation (with no rate feedback) which was so rapid that it was difficult to measure the amplitude ratio from the time history, which extends, at most, for one

cycle. Thus, the experimental results for one particular rate feedback setting ($K_{\dot{\theta}}$ = 0.044 sec) in two degrees of freedom were analyzed. It was assumed that the increment in pitch damping produced by this feedback gain was equal to that produced by the same gain setting at 80° duct incidence. This known increment in pitch damping is added to the value determined from the single-degree-of-freedom tests. Then the analysis proceeds as described. The dynamics of the vehicle with no feedback were then calculated from the resulting derivatives. The resulting characteristic roots agreed with the information that could be determined from measured transients. The increments in damping corresponding to other feedback settings agreed closely with those in the 80° case, as shown in Table IV. This confirms the assumption, inherent in this approach, that the moment produced per degree of differential fore and aft blade angle at i_d = 80° is equal to that at i_d = 70°.

i_d = 60°

It is necessary to add certain known terms to the equations of motion at i_d = 60° to account for the displacement of the cg of the model, with

respect to the pivot axis, as explained in Appendix I. Values of these terms, which were added to the equations of motion before proceeding with the analysis, are listed in Table IV. No alteration in the analysis procedure is required, since only known terms are added to the equations of motion.

In addition, a complication associated with the model control system was encountered at this flight condition. When the carriage was commanded by the model to accelerate to follow the model motion at these relatively high trim speeds, the increased current drawn by the carriage drive motor caused a noticeable drop in line voltage. This line-voltage drop affected a power supply in the model control system, producing a propeller blade angle change of equal value on all four propellers approximately proportional to carriage (model) acceleration. The configuration of the vehicle is such that total propeller blade angle change causes pitching moments (Reference 3), thus providing an apparent pitching moment variation with horizontal acceleration. It was assumed therefore that this effect could be accounted for by adding the unknown derivative $\Delta M_{\dot{u}_{ps}}$ to the analysis. It is then

possible to analyze the data, remove this effect, and determine the stability derivatives by an analysis similar to that described above.

Modifications to the model control system were made such that this coupling phenomenon was eliminated in the 50° duct incidence tests and all future tests.

i_d = 50°

The 50° case also required additional terms in the equations of motion to

13

include the effect of the displacement model cg from the pivot axis. Also, as mentioned earlier, no mechanical springs were used in the single-degree-of-freedom tests since the angle-of-attack stability derivative was negative ($M_w U_{o_f} < 0$). Otherwise, the analysis proceeds as described.

Table IV lists the stability derivatives found in model scale based on the inertia characteristics listed in Table III. The model scale derivatives are also shown graphically in Figure 12.

STABILITY DERIVATIVES OF THE FULL-SCALE AIRCRAFT

The stability derivatives determined for the model can be interpreted in terms of full-scale aircraft characteristics.

It is, of course, necessary to assume that there are no scale effects to make this interpretation. Comparison of the lift, drag, and pitching moments on an isolated duct of the model and the full-scale aircraft revealed that there were no appreciable scale effects on the model duct in the flight conditions of interest (Reference 1). Therefore, important scale effects are not expected to be present in the results.

Rather than present nondimensional derivatives, it is considered to be more convenient and conventional to present dimensional force derivatives divided by the mass of the aircraft, and pitching moment derivatives divided by the inertia. The full-scale derivatives are based on the moment of inertia of the Bell X-22A, as given in Reference 3.

The dimensional full-scale derivatives are listed in Table VI and are shown graphically in Figure 13 for the full-scale aircraft, using the altitude gross weight equivalence discussed in Appendix III. The relationship that applies for the test program is shown in Figure 14, and the conversion factors that result are given in Table V. Thus, for example, the derivatives presented correspond to the X-22A flying at a gross weight of 16,800 pounds at sea level or a gross weight of 14,000 pounds at a density altitude of 6000 feet.

The stability derivatives show the following trends.

THE SPEED STABILITY (M_u)

This derivative is large and positive at the three highest duct incidences tested; it decreases considerably at duct incidences of 60° and 50°. The large value near hovering and in low-speed flight is the primary source of the oscillatory instability present in the data; also it indicates that the vehicle will exhibit an appreciable sensitivity to horizontal gusts.

THE ANGLE-OF-ATTACK STABILITY ($M_w U_{o_f}$)

This derivative is fairly large and positive (unstable) at all but the lowest duct incidence tested. At a duct incidence of 50°, the derivative is negative. The unstable value of the derivative contributes to the instabilities of the motion at the higher duct incidences, and the change in sign is the primary contributor causing the stable motion at a duct incidence of 50°. The trend in this derivative is typical of V/STOL aircraft at low speeds.

THE PITCH DAMPING ($M_{\dot{\theta}}$)

This derivative is comparatively small and negative and generally increases with decreasing duct incidence. It is not clear at this time why the trend in this derivative does not follow a smooth curve. The low values indicate that the full-scale vehicle would require damping augmentation to provide satisfactory handling qualities at low speeds. The small value of this derivative may be seen by noting the large increments in damping (roughly a factor of 10 at duct incidences of 80° and 70°) required to make the transient motion neutrally stable.

THE DOWNWASH LAG ($M_{\dot{w}}$)

All indications from the data are that this derivative is small compared to the pitch damping.

THE RATE OF CHANGE OF HORIZONTAL FORCE WITH HORIZONTAL VELOCITY (X_u)

This derivative is large and negative at low speeds. The primary source of this derivative is the momentum drag of the ducts.

THE LIFT CURVE SLOPE (Z_w)

This derivative is small and increases with speed. The value of the derivative was not determined in hovering. The values at low speeds must be considered as approximate, since there is only weak coupling between the two-degree-of-freedom (θ-U_f) motion and the three-degree-of-freedom (θ-U_f-w_f) motion. This makes it difficult to determine Z_w accurately.

THE RATE OF CHANGE OF VERTICAL FORCE WITH HORIZONTAL VELOCITY (Z_u)

This derivative is small and of normal sign (negative) in the cases where it was evaluated.

THE RATE OF CHANGE OF HORIZONTAL FORCE WITH VERTICAL VELOCITY (X_w)

This derivative is normally small and was not determined from the experiments. It was assumed to be negligible in the analysis.

16

CONCLUSIONS AND RECOMMENDATION

CONCLUSIONS

1. The pitching moment derivatives of this quad configurat on V/STOL model exhibit the following characteristics:

   a. The speed stability (M_u) is large and positive (statically stable) at high duct incidences.

   b. The angle-of-attack stability ($M_w U_{o_f}$) is positive (unstable) at all but the lowest duct incidence tested (50°).

   c. The damping in pitch ($M_{\dot\theta}$) is stable but small in hover and increases with decreasing duct incidence.

2. For analysis of the data, the inclusion of test conditions with pitch rate feedback was valuable, particularly in the experiments where the basic model was highly unstable.

RECOMMENDATION

It is recommended that an effort be made to correlate the results obtained herein in the form of stability derivatives with full-scale flight-test data on similar configurations.

TABLE I. SUMMARY OF LONGITUDINAL TEST CONDITIONS AND MEASURED ROOTS

Duct Incidence i_d (deg)	Average Propeller Pitch $\beta_{.75R}$ (deg)	Differential Collective Pitch $\Delta\beta_o$ (deg)	Propeller Speed (rpm)	Trim Velocity U_{o_f} (ft/sec)	Degrees of Freedom	Stability Augmentation $K_{\dot\theta}$ (sec)	Roots of Oscillatory Motions s (1/sec)
90^c	25.8	0	7000	0	θ^b	0.044	
						0.030	-0.268 $\pm2.19i$
						none	
	29.2		6400			0.044	
						0.030	
						none	
	25.8		6400			0.044	
						0.030	
						none	
	25.8		0			0.044	-0.042 $\pm2.19i$
						0.030	
			7000		$\theta-U_f$	none	$+1.13$ $\pm1.67i$

18

TABLE I - Continued

Duct Incidence i_d (deg)	Average Propeller Pitch $\beta_{.75R}$ (deg)	Differential Collective Pitch $\Delta\beta_o$ (deg)	Propeller Speed (rpm)	Trim Velocity U_{o_f} (ft/sec)	Degrees of Freedom	Stability Augmentation $K_{\dot\theta}$ (sec)	Roots of Oscillatory Motions s (1/sec)
90[c]	25.8[a]	0	6400	0	$\theta-U_f$	none	+0.85 ±1.85i
	29.2						+1.03 ±1.83i
			0	11	θ[b,c]		-0.04 ±2.66i
				8	θ[b]		-0.266±2.42i / +1.38,-1.84[d]
80	25.2	1.9	6780	11	$\theta-U_f$		+1.06 ±1.74i
						0.030	+0.22 ±1.45i
						0.044	0±1.12i
						0.060	0±0.84i
	23.7	1.8			$\theta-w_f$	none	-
					$\theta-U_f-w_f$		+1.06 ±1.74i
70[e]	25.2	2.8	0	0	θ[b,c]		-0.29 ±2.61i
							-0.57±1.57i
			6780	22	θ[b]		-3.08,+2.12[d]

TABLE I - Continued

Duct Incidence i_d (deg)	Average Propeller Pitch $\beta_{.75R}$ (deg)	Differential Collective Pitch $\Delta\theta_o$ (deg)	Propeller Speed (rpm)	Trim Velocity U_{o_f} (ft/sec)	Degrees of Freedom	Stability Augmentation $K_{\dot\theta}$ (sec)	Roots of Oscillatory Motions s (1/sec)
70^e	26.2	6.0	6780	22	$\theta-U_f$	none	-
						0.021	-
						0.027	-
						0.030	+0.31 ±1.25i
						0.044	+0.05 ±1.04i
						0.060	-0.01 ±0.97i
					$\theta-w_f$	none	-
					$\theta-U_f-w_f$	0.021	-
						0.027	-
						0.030	+0.25 ±1.32i
60	25.5	4.1	0	0	$\theta^{b,c}$	none	-0.043 ±2.51i
			6780	28	θ^b	none	-0.33 ±2.09i +1.21, -1.75d

20

TABLE I - Concluded

Duct Incidence i_d (deg)	Average Propeller Pitch $\beta_{.75R}$ (deg)	Differential Collective Pitch $\Delta\beta_0$ (deg)	Propeller Speed (rpm)	Trim Velocity U_{o_f} (ft/sec)	Degrees of Freedom	Stability Augmentation $K_{\dot\theta}$ (sec)	Roots of Oscillatory Motions s (1/sec)
60	25.4	2.1	6780	28	$\theta-U_f$	none	+0.46 ±1.18i[f]
					$\theta-U_f$	0.027	-0.10 ±0.98i[f]
					$\theta-w_f$	none	—
					$\theta-U_f-w_f$		+0.28 ±1.48i[f]
50	25.3	2.5		36	$\theta\,g$		-0.432 ±2.58i
					$\theta-U_f$		0+2.24i
					$\theta-w_f$		-0.65 ±2.85i
					$\theta-U_f-w_f$		-0.93 ±2.74i

All tests at non-zero rpm conducted with Lift = 51.5 lb except as noted.

a. Lift = 43.1 lb
b. θ Freedom restrained with mechanical spring.
c. Model cg at pivot axis.
d. Calculated roots with mechanical spring removed.

e. Figures 17 through 28.
f. See text for interpretation of these data.
g. No mechanical spring used.

TABLE II.	SCALE FACTORS FOR DYNAMIC MODEL SIMILARITY	
Multiply full-scale property by scale factor to obtain model property.		
		For $\lambda_t = 0.1463$
Linear dimension	λ_t	0.1463
Area	λ_t^2	2.112×10^{-2}
Volume, mass, force	λ_t^3	3.071×10^{-3}
Moment	λ_t^4	4.463×10^{-4}
Moment of inertia	λ_t^5	6.487×10^{-5}
Linear velocity	$\lambda_t^{0.5}$	0.3812
Linear acceleration	λ_t^0	1.000
Angular velocity	$\lambda_t^{-0.5}$	2.623
Angular acceleration	λ_t	0.1463
Time	$\lambda_t^{0.5}$	0.3812
Frequency	$\lambda_t^{-0.5}$	2.623
Reynolds number	$\lambda_t^{1.5}$	5.591×10^{-2}
Mach number	$\lambda_t^{0.5}$	0.3812

where $\lambda_t = \dfrac{\text{model linear dimension}}{\text{full-scale linear dimension}}$

TABLE III. MODEL GEOMETRIC AND INERTIA CHARACTERISTICS

Model Height = 11.5 lb

Duct Incidence i_d (deg)	Pivot Axis Location x_{pivot} (FS)	Pivot Axis Location z_{pivot} (WL)	Location of cg Relative to Pivot x_{cg} (in.)	Location of cg Relative to Pivot z_{cg} (in.)	Moment of Inertia About Pivot Axis I_y (slug-ft²)	Mechanical Spring Rate k_m (ft-lb/rad)	Propeller Rotational Speed (rpm)
90	45.30	20.20	0	0	2.52	31.1*	0, 6400, and 7000
80	45.70	20.10	0	0	2.05	none	6400, 7000
					2.82	18.1*	0
			2.47	0.37	2.44	18.1*	6780
	44.45	20.10	0	0	2.25	none**	0
70						18.1*	
	45.70	20.10	0	0.38	2.80	62.8*	6780
						18.1*	
			2.55	0.48	2.15	62.8*	
	44.45	20.10	0	0	2.23	none**	
60			0	0.60	3.17	18.1*	0
	45.70	20.10	2.47	0.60	2.63	18.1*	6780
						none**	
50	45.70	20.10	2.56	0.67	2.63	none	

*Single-degree-of-freedom runs only.
**Multiple degree-of-freedom runs only.

23

	Duct Incidence (deg)				
	90	80	70	60	50
Model Trim Velocities and Aerodynamic Derivatives					
U_{o_f}, ft/sec	0	10	22	28	36
X_u, 1/sec	-.53	-.45	-.70	-.60	-.50
X_v, 1/sec	Assumed Negligible in all Cases				
Z_u, 1/sec	Neg	Neg	-.19	-.655	-.830
Z_v, 1/sec	NA	NA	-.14	-.675	-.895
M_u, 1/ft-sec	+.307	+.421	+.484	+.157	+.154
M_v, 1/ft-sec	NA	+.255	+.297	+.110	-.160
$M_{\dot\theta}$, 1/sec	-.44	-.48	-.955	-.54	-.864
Additional Stability Derivatives Due to cg Offset					
$\Delta M_{\dot u_{cg}}$, 1/ft	0	0	0	-.0304	-.034
$\Delta M_{\dot v_{cg}}$, 1/ft	0	0	0	+.125	+0.13
$\Delta M_{\theta_{cg}}$, 1/sec²	0	C	0	-.98	-1.09
Additional Stability Derivatives Due to Stability Augmentation					
$\Delta M_{\dot\theta}$, 1/sec					
$K_{\dot\theta}$ = .027	NT	NT	NT	-2.59	NT
$K_{\dot\theta}$ = .030	NT	-4.37	-4.35	NT	NT
$K_{\dot\theta}$ = .044	NT	-8.15	-8.15	NT	NT
$K_{\dot\theta}$ = .060	NT	-11.9	-11.02	NT	NT
$\Delta M_{\dot u_{ps}}$, 1/ft	0	0	0	+.075	0

TABLE IV. MODEL STABILITY DERIVATIVES FOR TRIMMED LEVEL FLIGHT

Abbreviations: NA   Not Available
                 Neg Negligible
                 NT   Not Tested

Test Conditions given in Table I
Inertia Characteristics given in Table III
Trim Conditions given in Figure 8

TABLE V. INTERPRETATION OF FORCES, MOMENTS, AND VELOCITIES AT
OTHER GROSS WEIGHTS

	Altitude Gross Weight	Velocity Gross Weight
Forces	Λ_w	Λ_w
Moments	Λ_w	Λ_w
Velocities, angular and linear	1	$\Lambda_w^{.5}$
Air density	Λ_w	1
Angles	1	1

where $\Lambda_w = \dfrac{W_D}{W_C} = \dfrac{\text{desired gross weight}}{\text{gross weight determined by dynamic scaling}}$

To determine aerodynamic quantities at other gross weights, multiply
dynamic scaling results by the above quantities.

NOTE: Use of the first column results in no change in dynamic stability
characteristics. Use of the second column results in changes in
dynamics.

25

TABLE VI. FULL-SCALE STABILITY DERIVATIVES FOR TRIMMED LEVEL FLIGHT

	Duct Incidence (deg)				
	90	80	70	60	50
U_{o_f}, ft/sec	0	26.2	57.5	73.4	94.2
X_u, 1/sec	-.20	-.17	-.27	-.23	-.19
X_w, 1/sec	Assumed Negligible				
Z_u, 1/sec	Neg	Neg	-.073	-.25	-.32
Z_w, 1/sec	NA	NA	-.054	-.26	-.34
M_u, 1/ft-sec	+.017	+.026	+.028	+.011	+.011
M_w, 1/ft-sec	NA	+.015	+.017	+.0077	-.0112
$M_{\dot{\theta}}$, 1/sec	-.17	-.20	-.40	-.26	-.42

Abbreviations: NA   Not Available
                Neg Negligible

See Figure 14 for density altitude/gross weight correspondence.
Radius of gyration k_y = 8.5 ft.

26
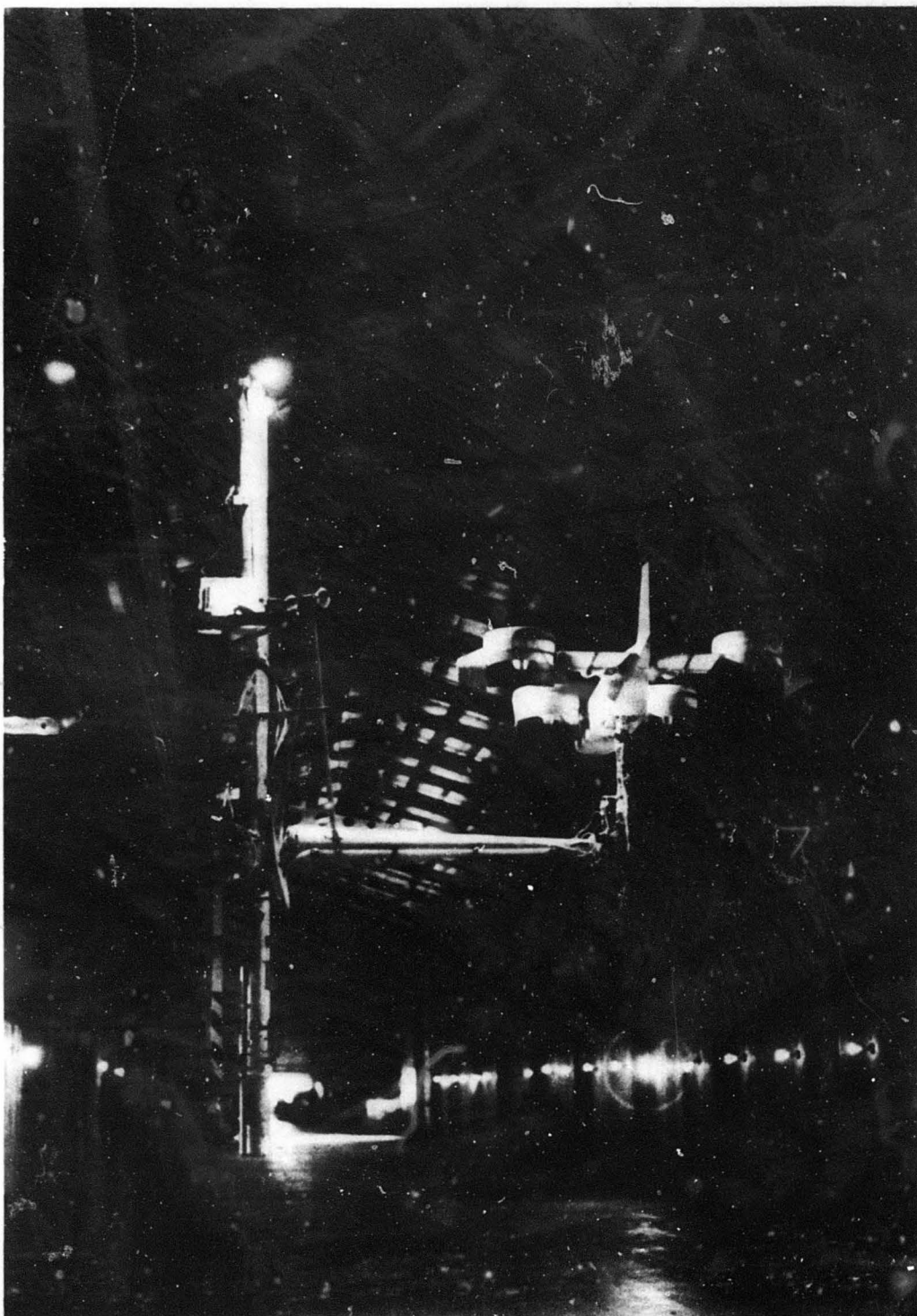
Figure 1. Princeton Dynamic Model Track - Model Mounted
on Longitudinal Dynamic Testing Apparatus.

27
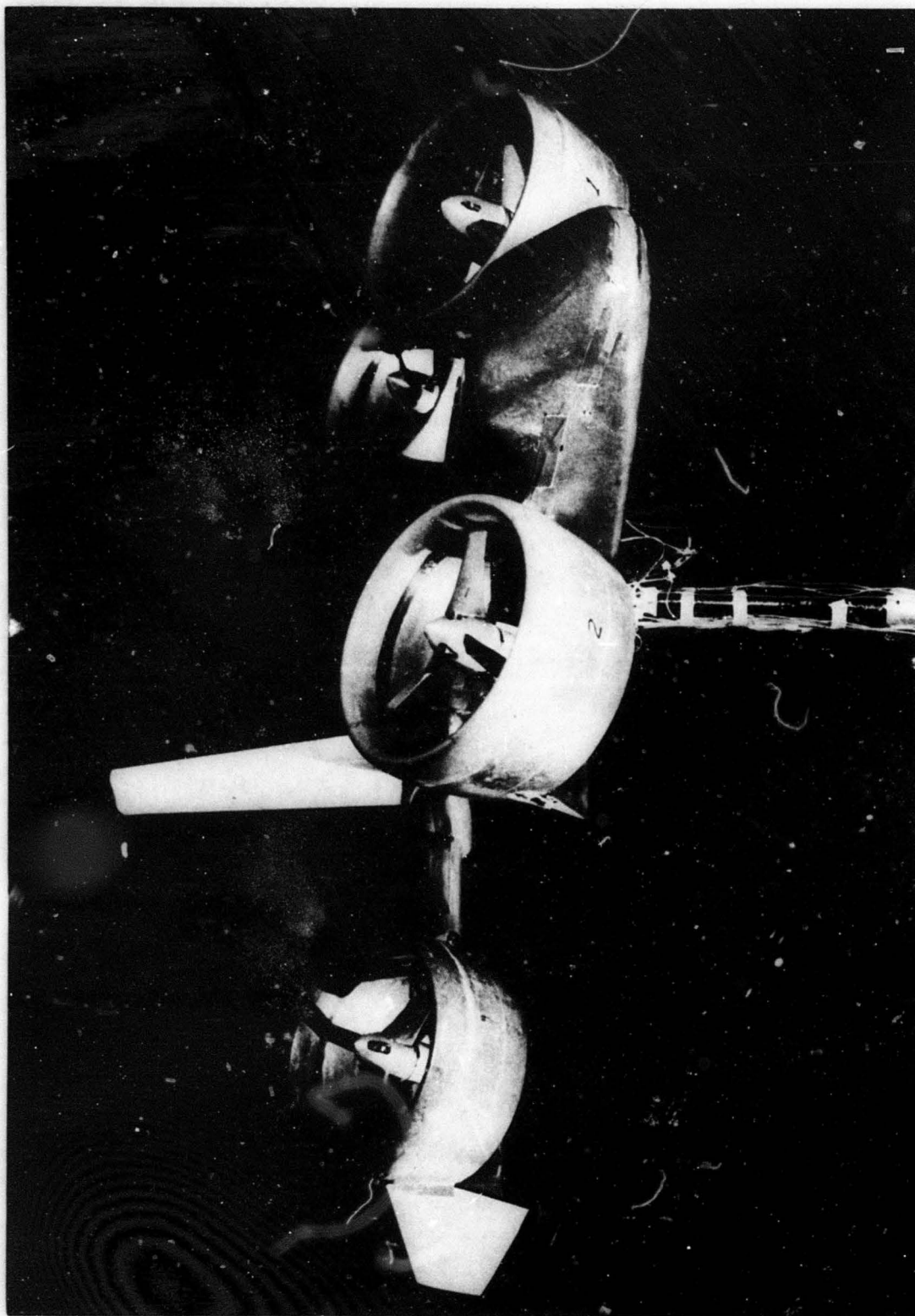
Figure 2. 0.145 Scale Quad Configuration Dynamic Model.
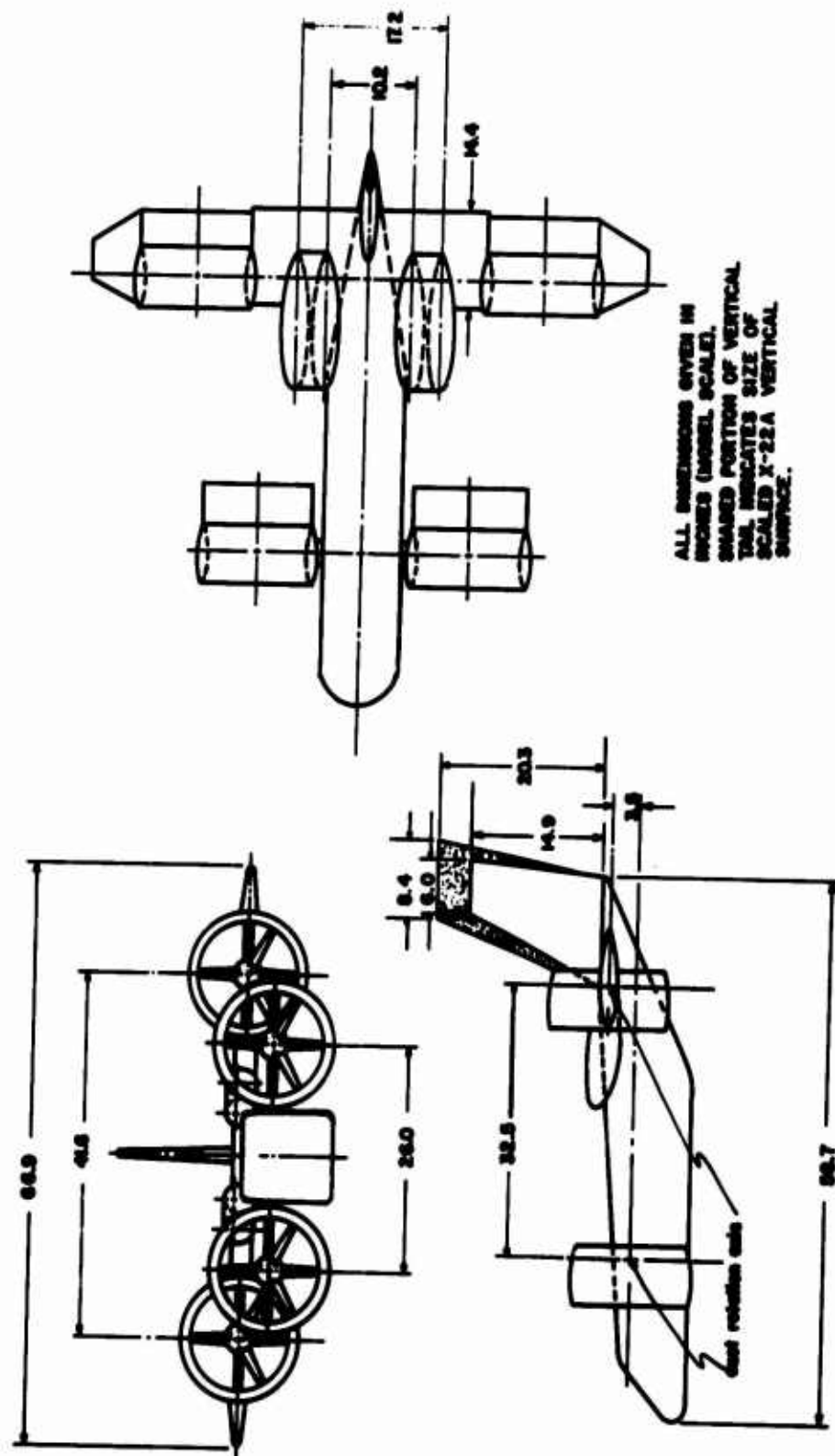
Figure 3. General Arrangement Drawing of Quad Model in X-22A Configuration.

ALL DIMENSIONS GIVEN IN
INCHES (MODEL SCALE).
SHADED PORTION OF VERTICAL
TAIL INDICATES SIZE OF
SCALED X-22A VERTICAL
SURFACE.

29

Figure 4. Location of Model Reference Stations and cg.
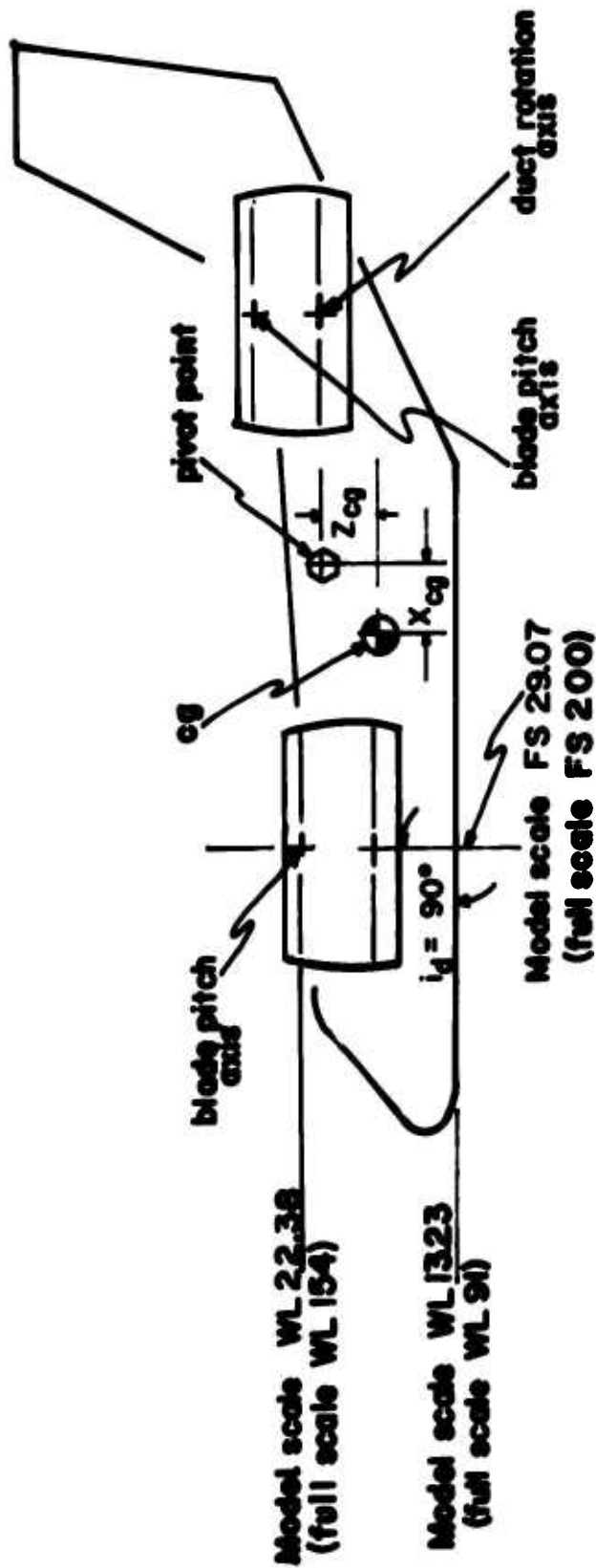
Note: 1. Reference FS and WL locations shown do not change with duct rotation.

2. Pivot point is reference point for aerodynamic measurements of complete aircraft.

3. Model angular motions measured about pivot point.
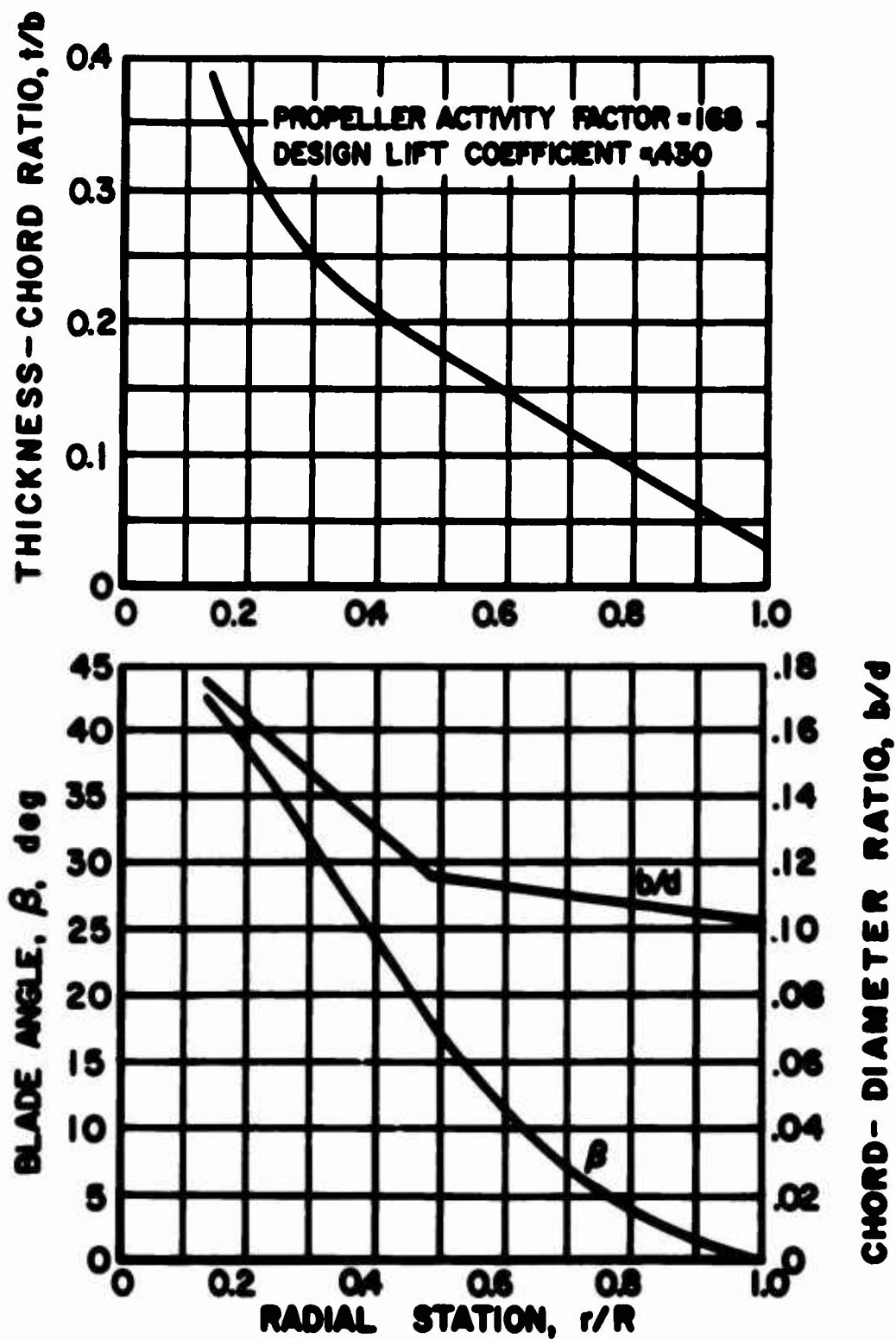
Figure 5. Geometric Characteristics of Three-Bladed Model Propellers.

31
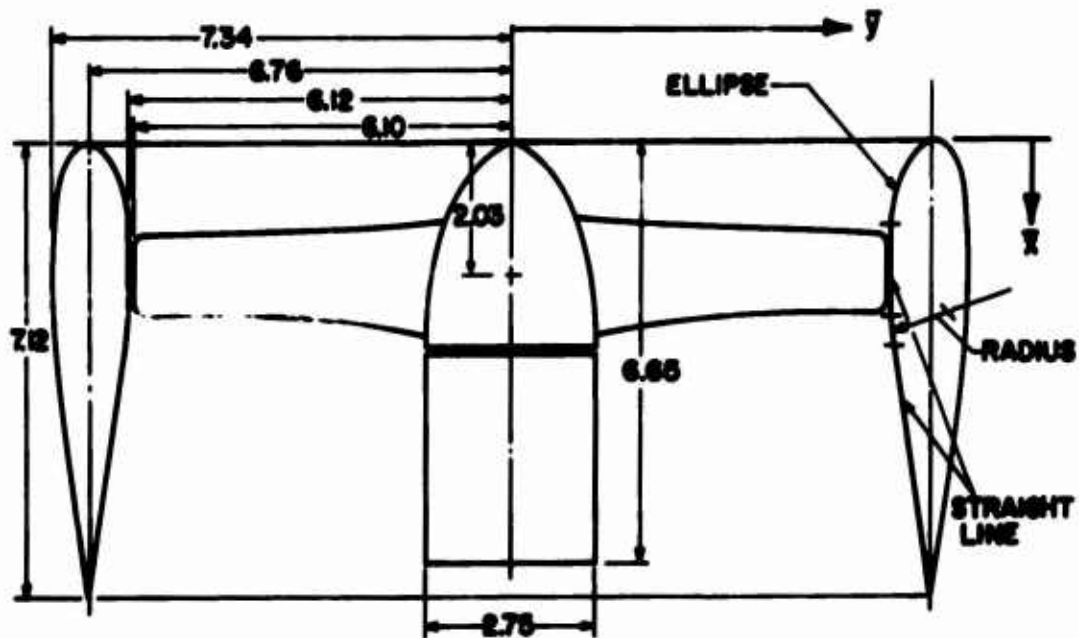
ALL DIMENSIONS ON ABOVE
DRAWING IN INCHES
(MODEL SCALE)

Figure 6. Geometric Characteristics of Scaled Model Ducts.

Figure 7. Geometric Characteristics and Reference Locations for Model Duct System

33
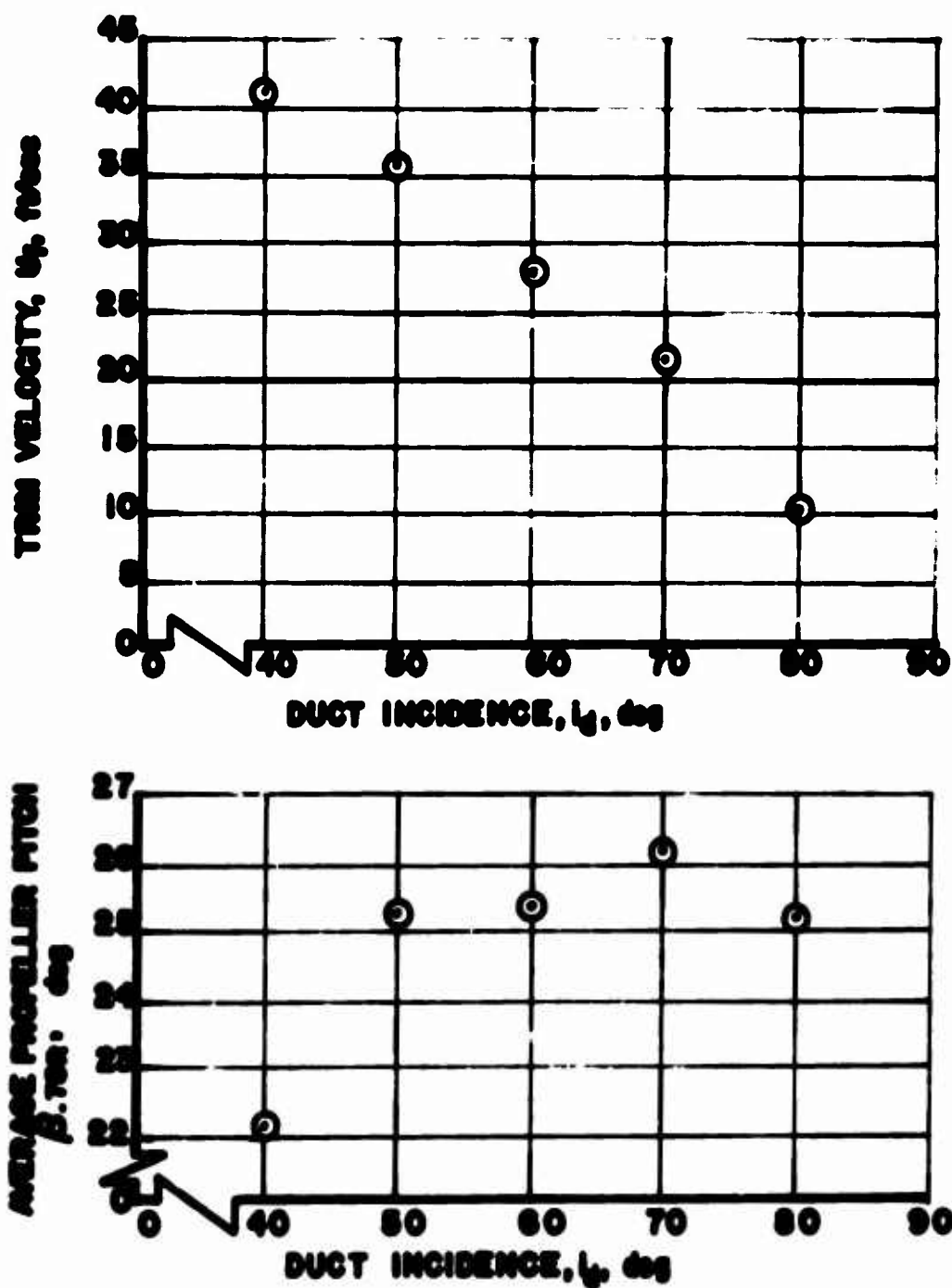
Figure 8.   Experimental Data, Model Trim Conditions -
Model Lift = Model Weight = 51.5 lb, rpm = 6780.

$u_f = u \cos \theta_o + w \sin \theta_o$

$w_f = -u \sin \theta_o + w \cos \theta_o$

MODEL
PIVOT AXIS

SPACE AXIS

NOTE: $X_f - Y_f$ PLANE
IS HORIZONTAL

TRANSLATIONAL
VELOCITIES ARE
SPACE-FIXED

FUSELAGE REFERENCE AXIS
(perturbed position)
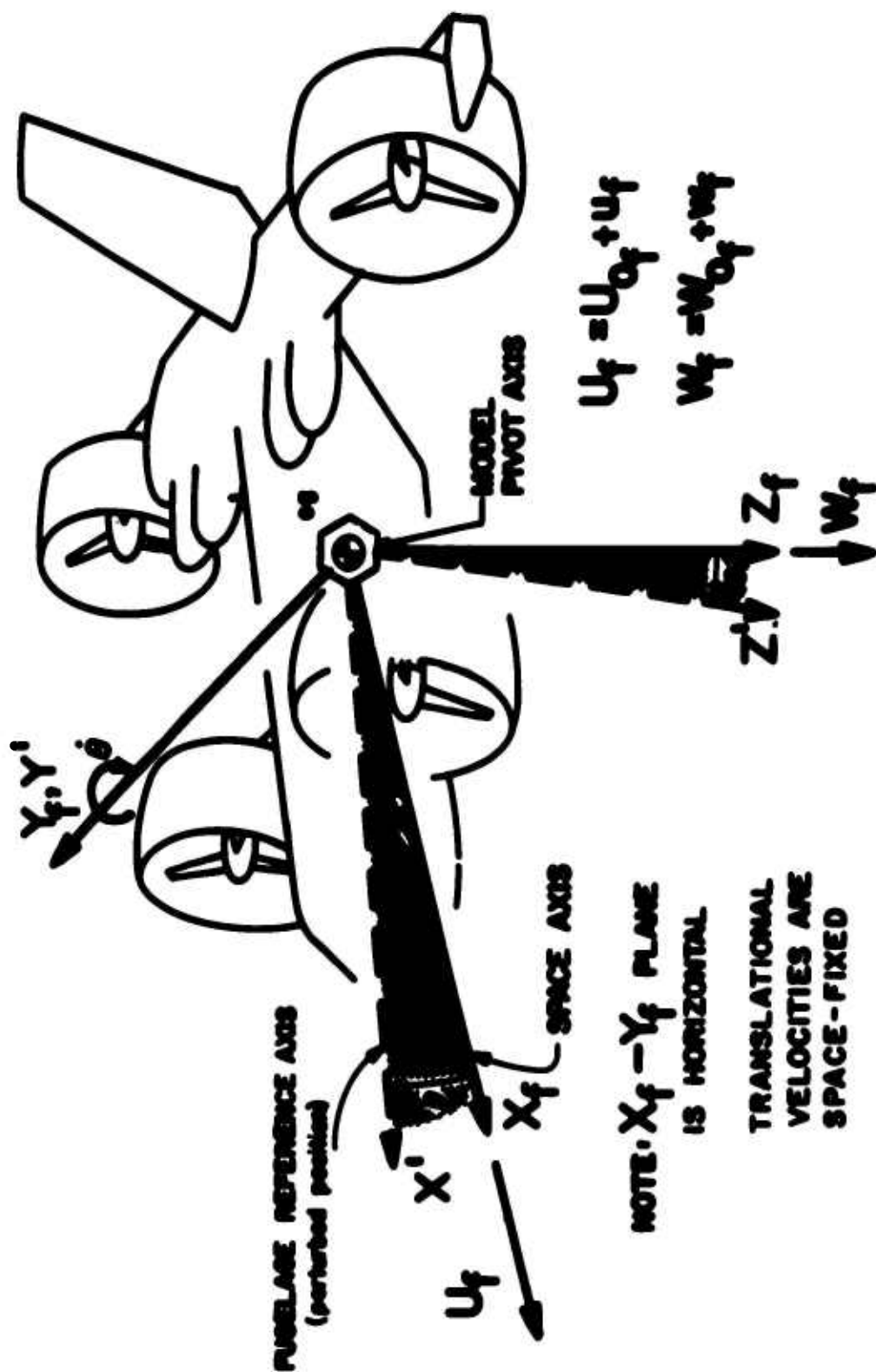
Figure 9. Axis System for Longitudinal Transient Response Data.
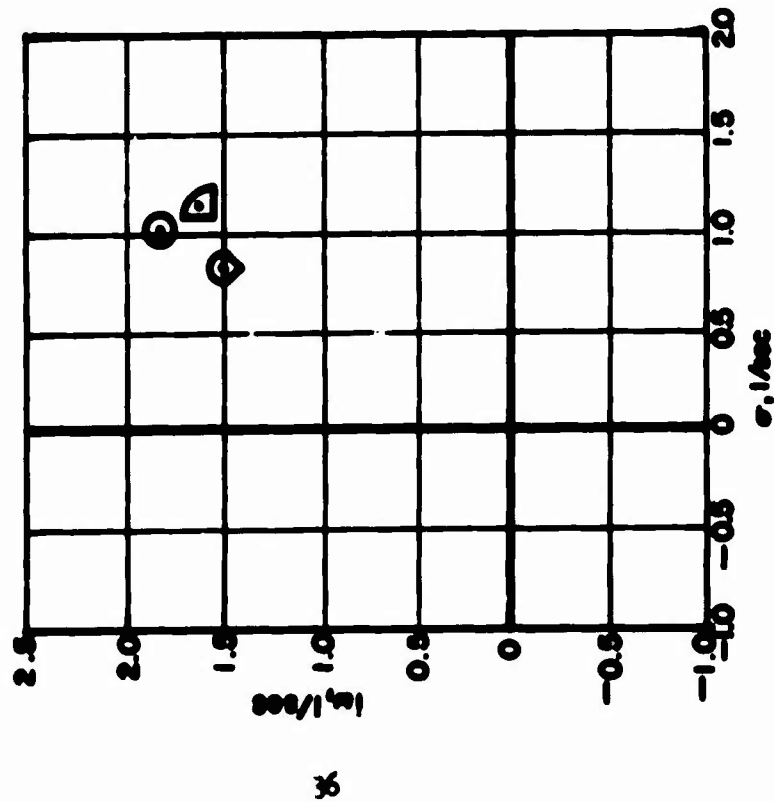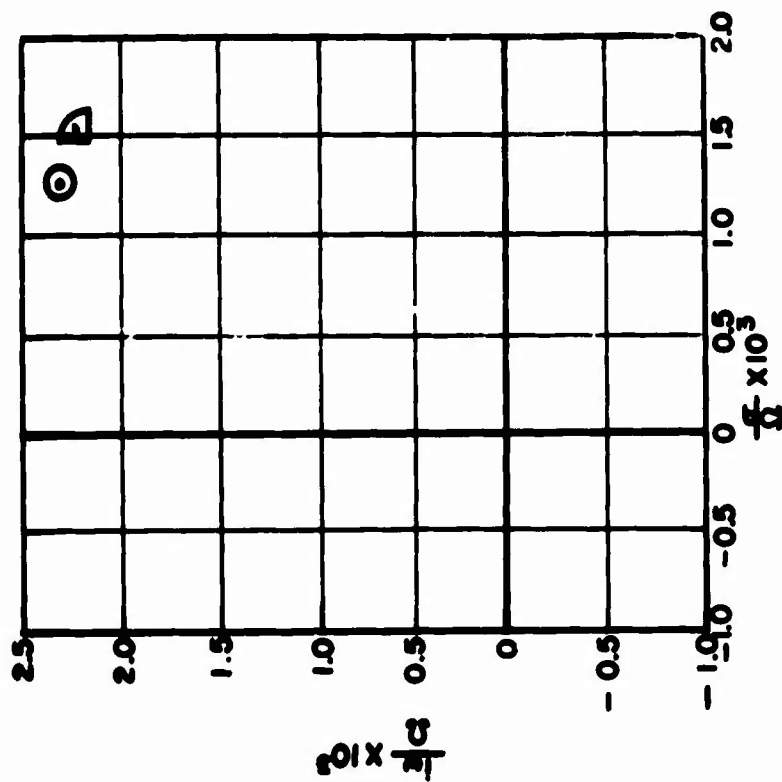
Figure 10. Experimentally Measured Transient Response Characteristics.

id = 80°

TWO DEGREES OF FREEDOM: $\theta - u_f$

⊙ NO STABILITY AUGMENTATION

⊙ $K_\theta' = 0.030$ sec

⊙ $K_\theta' = 0.044$ sec

⊙ $K_\theta' = 0.060$ sec
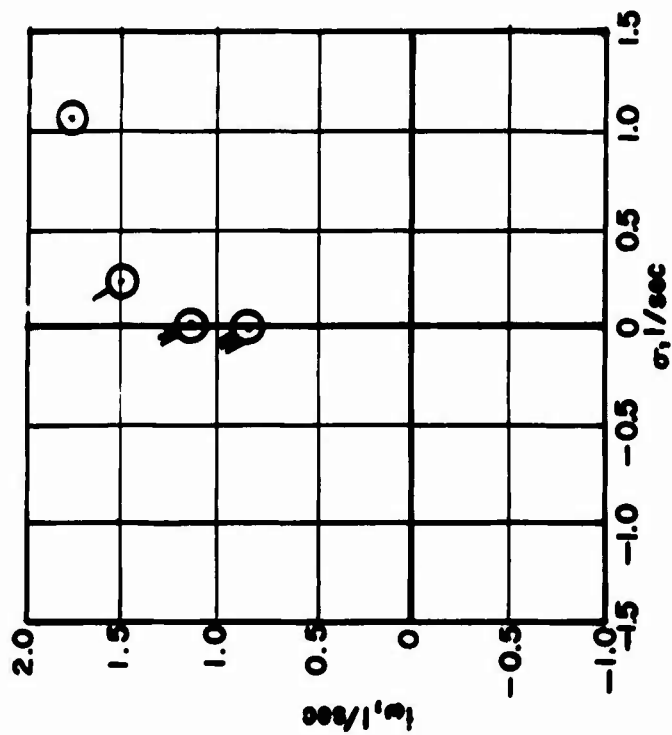
$\sigma, 1/sec$

$|\omega|, 1/sec$

$\psi = 80°$, NO STABILITY AUGMENTATION

▲ ONE DEGREE OF FREEDOM: θ

⊙ TWO DEGREES OF FREEDOM: $\theta - u_f$

☐ THREE DEGREES OF FREEDOM: $\theta - u_f - w_f$

$\sigma, 1/sec$

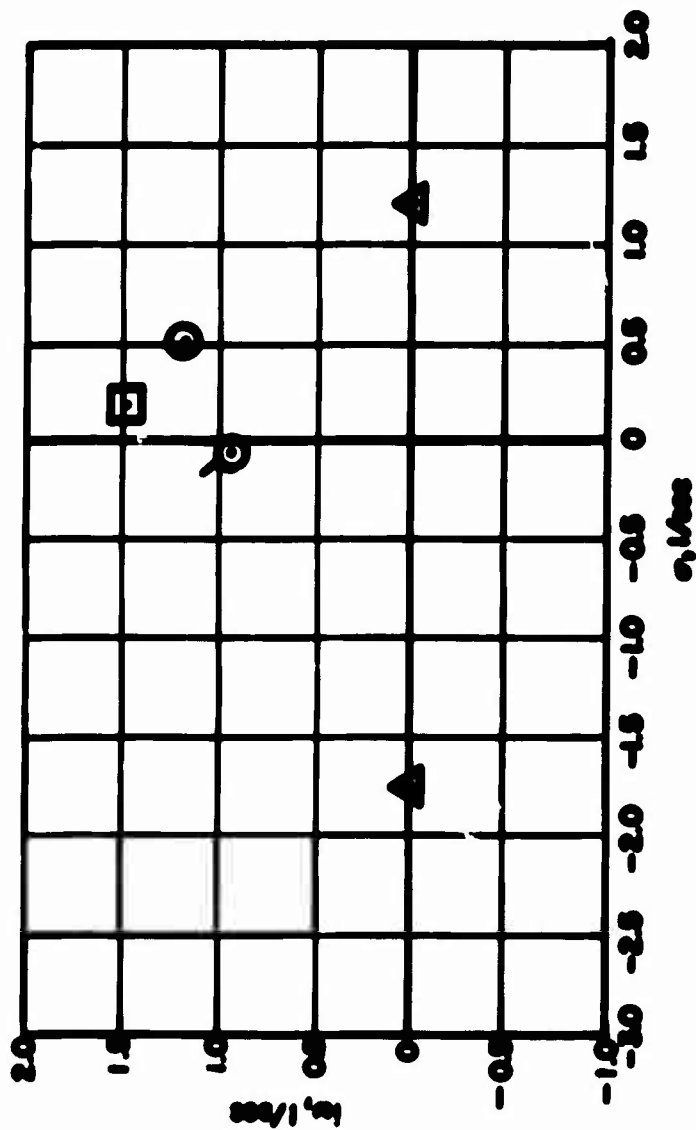$|\omega|, 1/sec$

Figure 10. Continued.

Figure 10. Continued

Figure 10. Continued

39
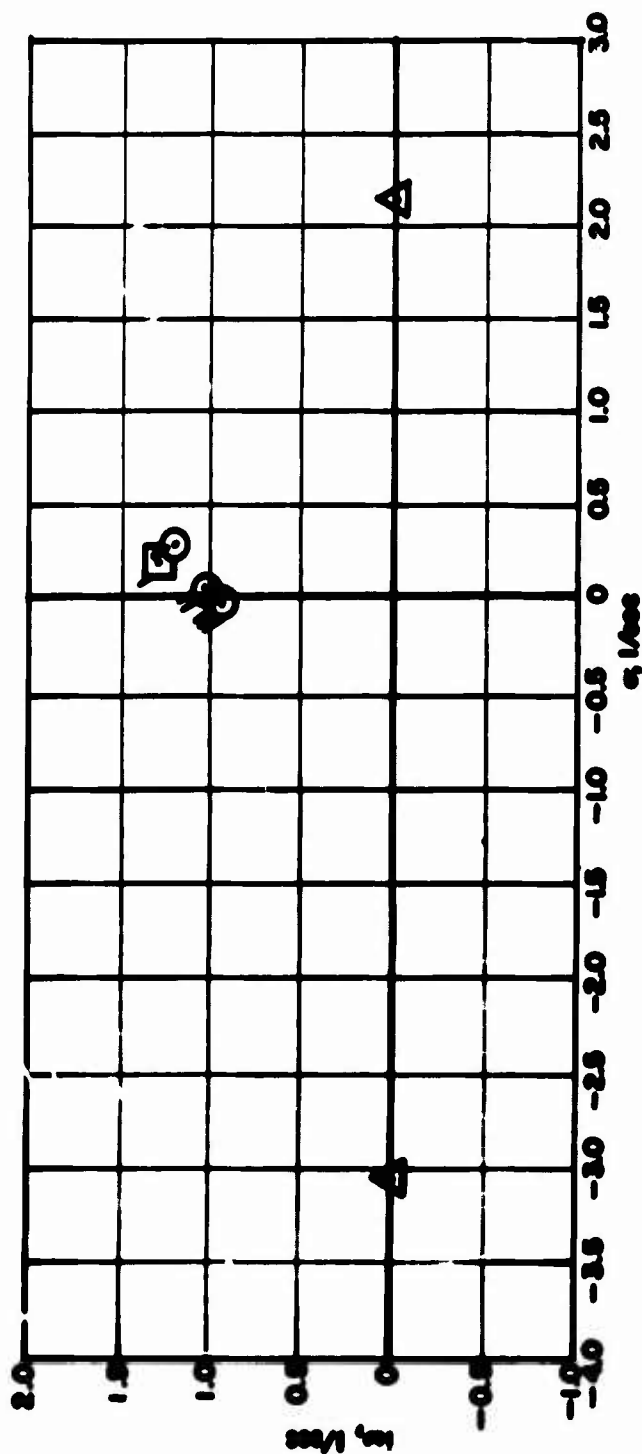
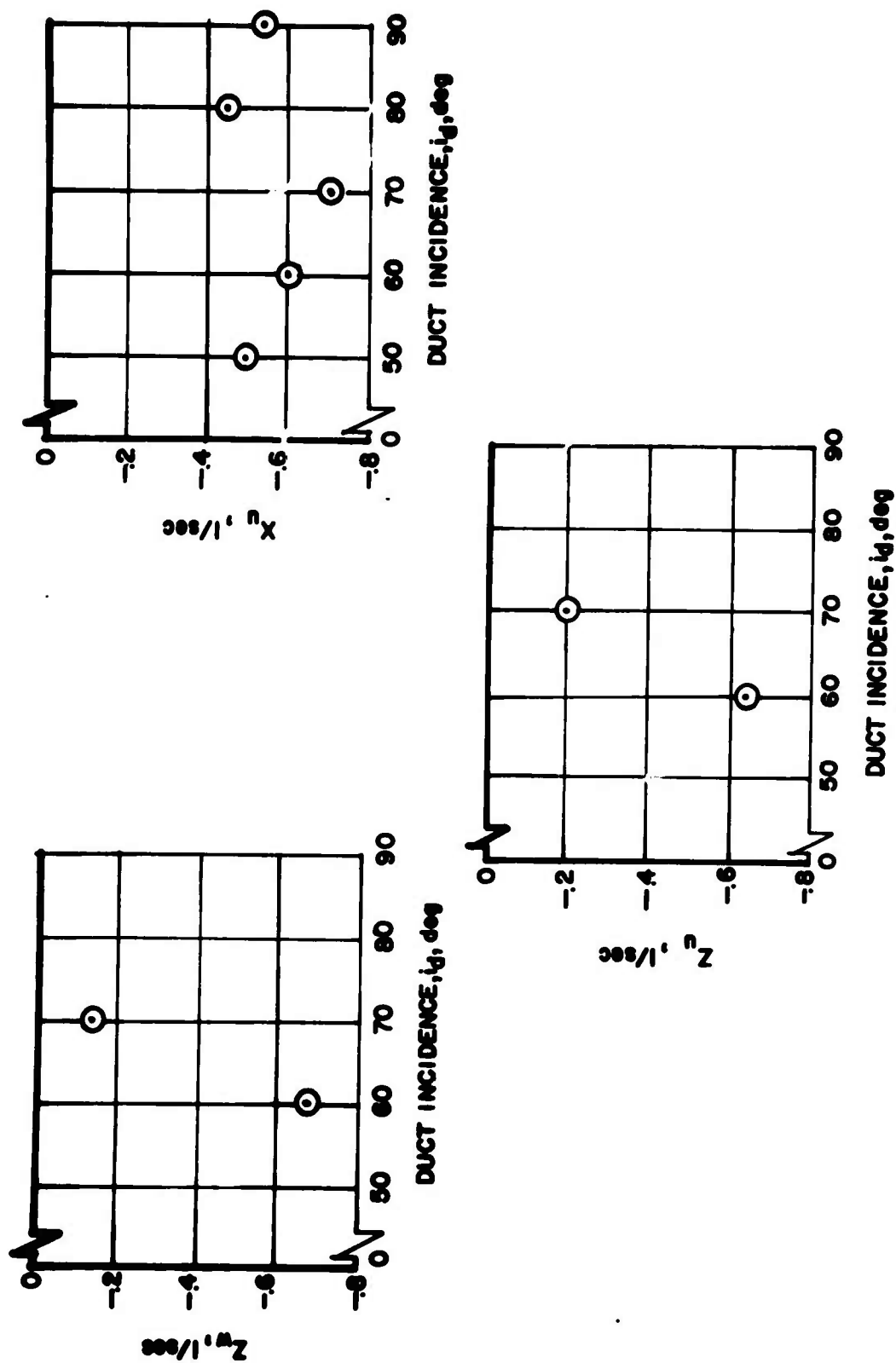Figure 12. Model Stability Derivatives for Trimmed Level Flight.
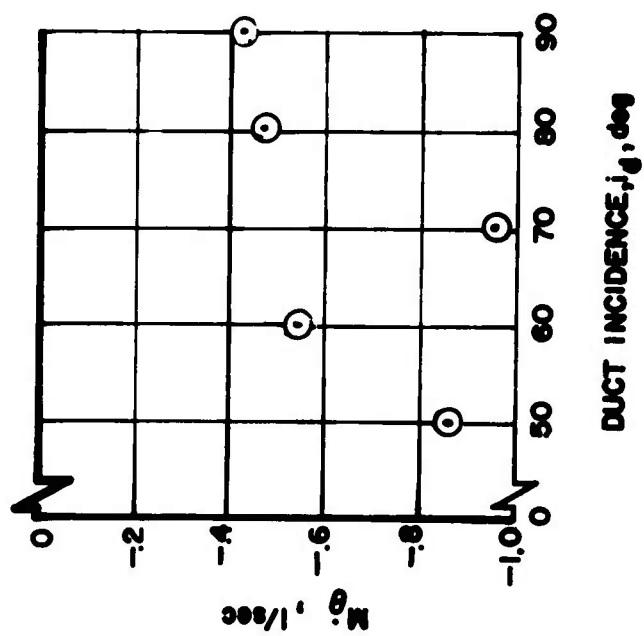
Figure 12. Concluded.

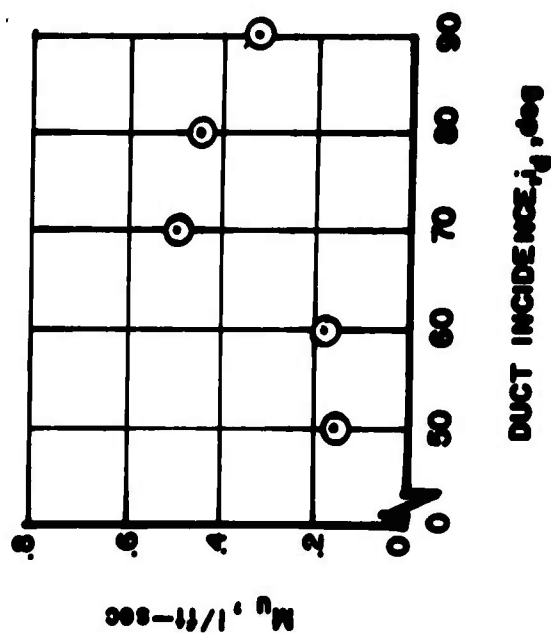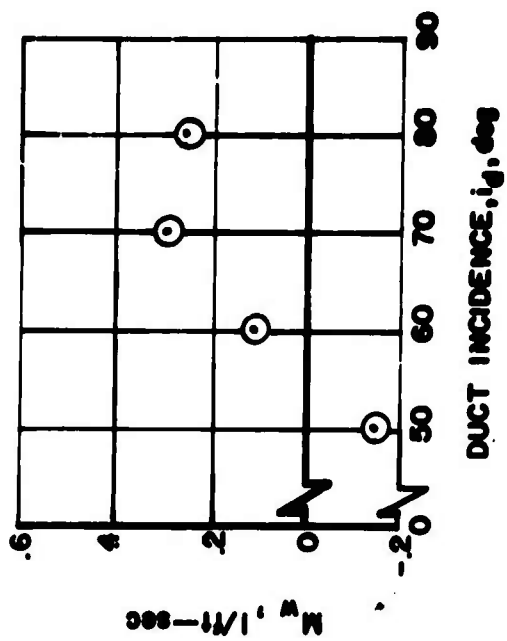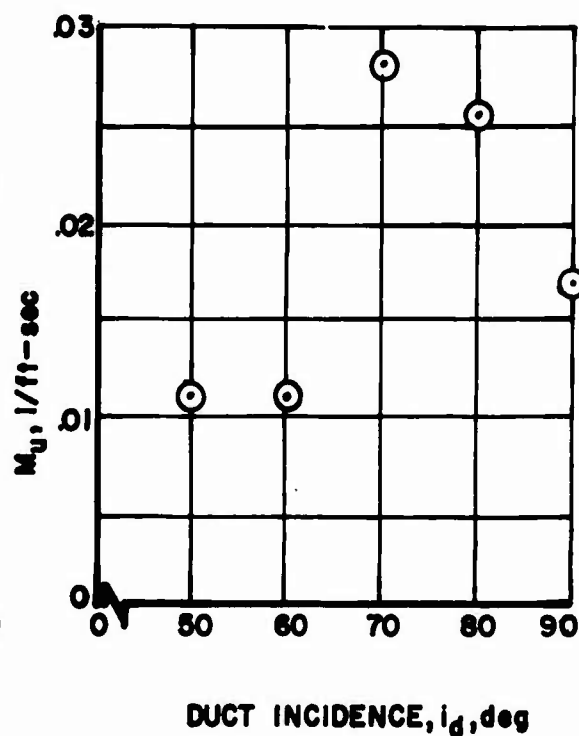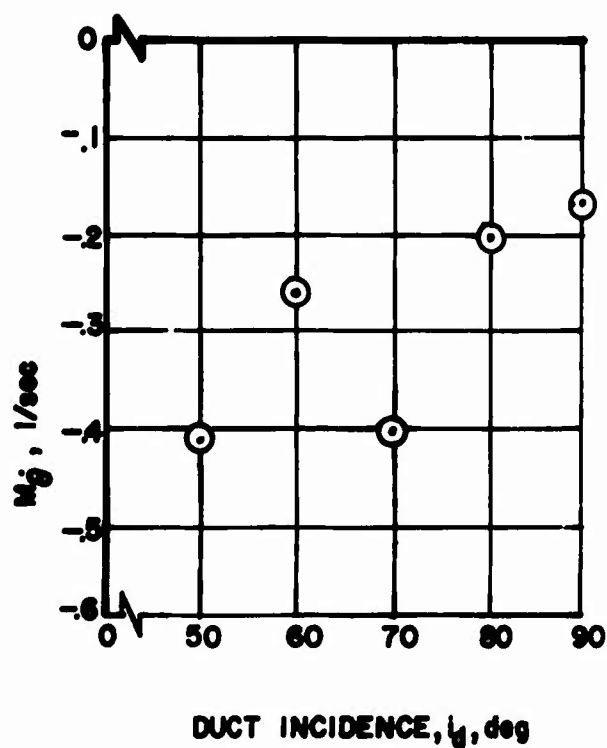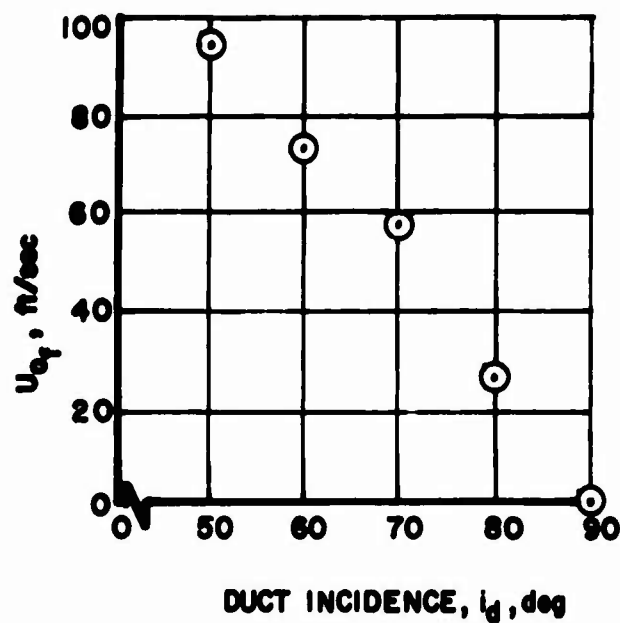Figure 13. Full-Scale Stability Derivatives and Trim Condition for
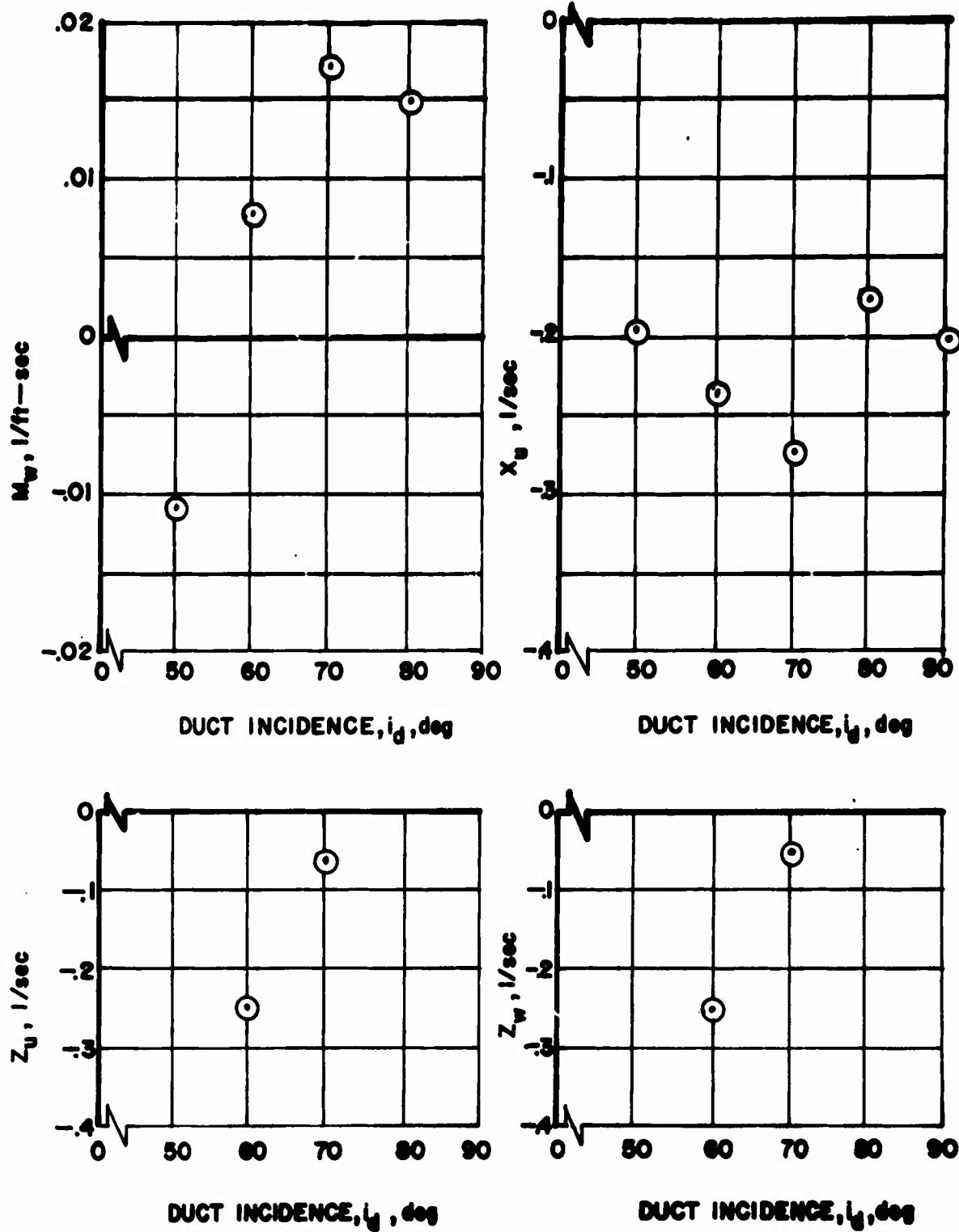Altitude/Gross Weight Correspondence Shown in Figure 14
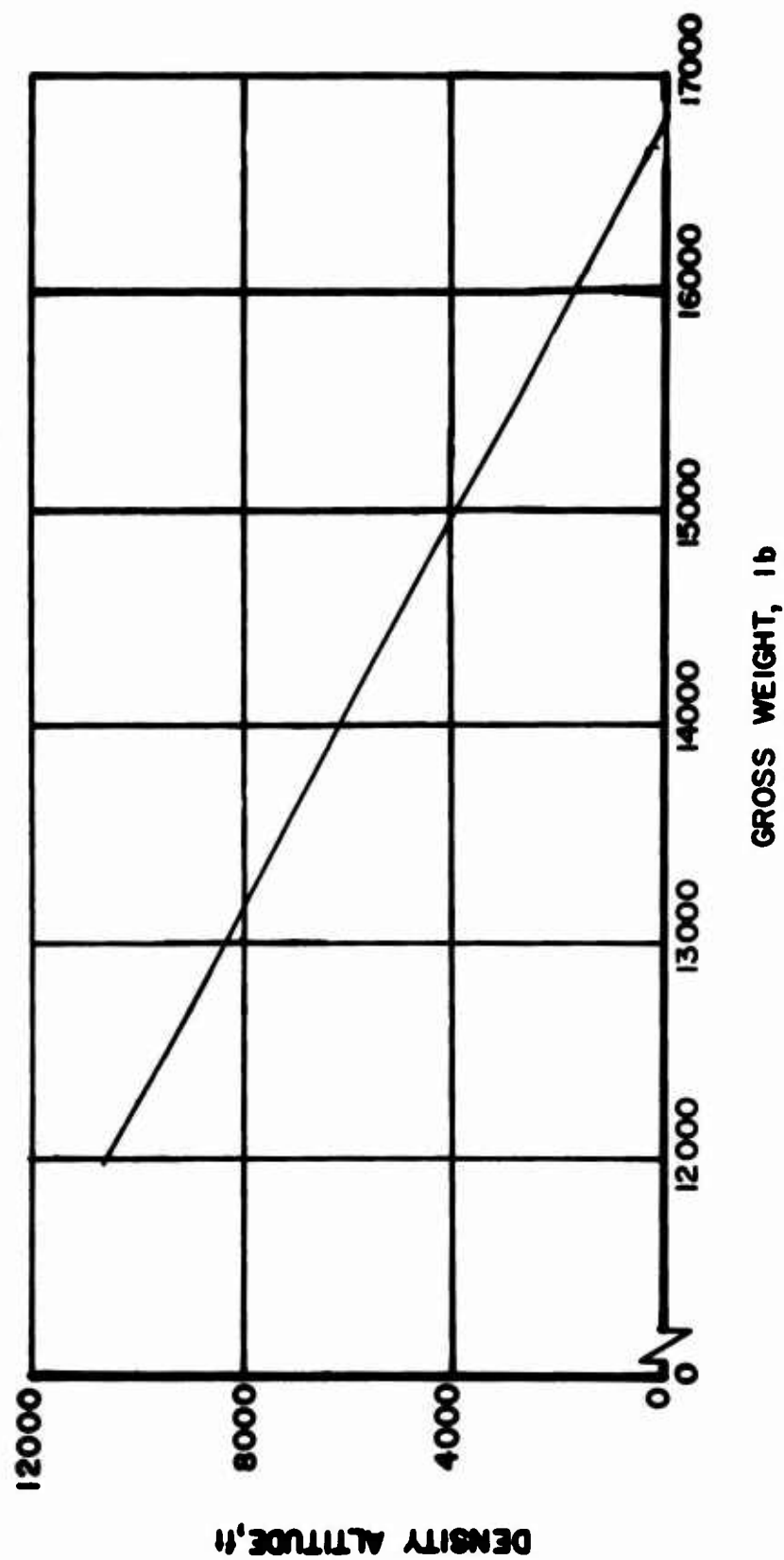($k_y = 8.5$ ft).

44

Figure 13. Concluded.

45

Figure 14. Density Altitude/Gross Weight Correspondence for Stability Derivatives.

REFERENCES

1. Putman, W. F., Traybar, J. J., Curtiss, H. C., Jr., and Kukon, J. P.,
   AN INVESTIGATION OF THE DYNAMIC STABILITY CHARACTERISTICS OF A QUAD
   CONFIGURATION, DUCTED-PROPELLER V/STOL MODEL, Volume I, Phase I -
   Hovering Data Report, Princeton University; USAAVLABS Technical Report
   68-49A, U. S. Army Aviation Materiel Laboratories, Fort Eustis,
   Virginia, September 1968.

2. Putman, W. F., Traybar, J. J., Curtiss, H. C., Jr. and Kukon, J. P.,
   AN INVESTIGATION OF THE DYNAMIC STABILITY CHARACTERISTICS OF A QUAD
   CONFIGURATION, DUCTED-PROPELLER V/STOL MODEL, Volume II, Phase II -
   Longitudinal Dynamics at High Duct Incidence Data Report, Princeton
   University; USAAVLABS Technical Report 68-49B, U. S. Army Aviation
   Materiel Laboratories, Fort Eustis, Virginia, August 1968, AD 676861.

3. Michaels, J. L., and Hesby, A. T., AERODYNAMIC STABILITY AND CONTROL
   AND FLYING QUALITIES, X-22A, Bell Aerosystems Company Report No.
   2127-917003, Division of Bell Aerospace Corporation, Buffalo, New York,
   December 1962.

4. Curtiss, H. C., Jr., Putman, W. F., and Traybar, J. J., GENERAL
   DESCRIPTION OF THE PRINCETON DYNAMIC MODEL TRACK, Princeton University;
   USAAVLABS Technical Report 66-73, U. S. Army Aviation Materiel
   Laboratories, Fort Eustis, Virginia, November 1966, AD 645 883.

5. Putman, W. F., SPECIFICATIONS FOR DESIGN OF A VARIABLE CONFIGURATION
   QUAD MODEL, Princeton University; Department of Aerospace and
   Mechanical Sciences Report 839, Princeton, New Jersey, October 1965.

6. Seckel, Edward, STABILITY AND CONTROL OF AIRPLANES AND HELICOPTERS,
   New York, Academic Press, 1964.

Linearized equations of motion, applicable to the analysis of various experimentally measured responses, are presented in this appendix.

The longitudinal equations of motion that describe the small perturbation motion of an aircraft from initially level flight, using a stability axis system (Reference 6), are.

$$\dot{u} - X_u u - X_w w + g\theta = 0$$

$$\dot{w} - Z_w w - Z_u u - U_o \dot{\theta} = 0$$

$$M_w w + M_{\dot{w}} \dot{w} + M_u u + M_{\dot{\theta}} \dot{\theta} - \ddot{\theta} = 0 \tag{10}$$

Two derivatives $X_{\dot{\theta}}$ and $Z_{\dot{\theta}}$ that are usually small are neglected.

Since all of the transient responses were measured and are presented in terms of space-fixed variables, it is convenient to transform equations (10) to a space-fixed system (Figure 15), with the X_f axis parallel to the horizon, by the following transformations:

$$u = u_f - W_{o_f}\theta$$

$$w = w_f + U_{o_f}\theta \tag{11}$$

where W_{o_f} is equal to zero from the condition of initially level flight.

Substituting the relationships of equation (11) into equations (10), the following equations result:

$$\dot{u}_f - X_u u_f - X_w w_f + (g - X_w U_{o_f})\theta = 0$$

$$\dot{w}_f - Z_w w_f - Z_u u_f - Z_w U_{o_f}\theta = 0$$

$$\ddot{\theta} - (M_{\dot{\theta}} + M_{\dot{w}}U_{o_f})\dot{\theta} - M_w U_{o_f}\theta - M_u u_f - M_{\dot{w}}\dot{w}_f - M_w w_f = 0 \tag{12}$$

Because of certain features of the model and the apparatus, three modifi- cations to these equations are necessary such that they will apply to all test conditions.

1. There are two linkages required to attach the model to the force transducers and mounting system used for this type of testing. These supports provide the horizontal and vertical translational degrees of freedom and contribute additional masses (m_h and m_v) that "fly" <u>along with the model</u> and, therefore, must be acceler- ated by the model. The two linkages are relatively light in weight compared to the "flying" weight of the model but never- theless should be accounted for by additional mass terms in the equations of motion. Generally, the arrangement and weights of these two supports are such that the mass accelerated by the model in the horizontal direction is larger than that accelerated in the vertical direction. If m_p is the total mass of the model resting on the pivot axis (Figure 16), then the total lifted mass of the model m when "flying" is equal to m_p plus the mass of the vertical link m_v or $m = m_p + m_v$. Similarly, the total accelerated mass in the horizontal direction m_t is equal to $m_p + m_v + m_h$ or $m + m_h$. This dynamic model mount characteristic requires the modification of all terms in the horizontal force equation, except the acceleration term, by a mass ratio defined as m/m_t and equal to 0.936 in value.

2. In certain of the test conditions, as indicated in Table III, the cg of the model was not located at the pivot axis of the model. Equations (12) may be considered to be written about the pitch pivot axis of the model, which represents the full-scale cg position about which the derivatives are determined. Additional terms are necessary in the equations of motion to account for the displacement of the model's cg. These are:

$$\Delta M_{\dot{u}_{cg}} = - \frac{z_{cg}\, m_p}{I_y}$$

$$\Delta M_{\dot{w}_{cg}} = \frac{x_{cg}\, m_p}{I_y}$$

$$\Delta M_{\theta_{cg}} = - \frac{W_p\, z_{cg}}{I_y} \tag{13}$$

where m_p and W_p are respectively the pivoting mass and pivoting weight of the model.

3. In certain of the tests (single degree of freedom only), a mechanical spring was added about the model pitch axis to provide a restoring moment which produces an oscillatory motion of the model. In these experiments the following term should be added:

$$\Delta M_{\theta_m} = - \frac{k_{\theta_m}}{I_y} \qquad (14)$$

In the experiments where a spring was employed, the value of the spring constant, k_{θ_m}, is as given in Table III.

Adding the necessary terms to account for these three effects, the complete equations of motion that apply to the measured transients obtained in this facility are:

$$\dot{u}_f - \frac{m}{m_t} X_u u_f - \frac{m}{m_t} X_w w_f + \frac{m}{m_t} (g - X_w U_{o_f}) \theta = 0$$

$$\dot{w}_f - Z_w w_f - Z_u u_f - Z_w U_{o_f} \theta = 0$$

$$\ddot{\theta} - (M_{\dot\theta} + M_{\dot w} U_{o_f}) \dot{\theta} + \left(\frac{k_{\theta_m}}{I_y} - M_w U_{o_f} + \frac{W_p z_{cg}}{I_y} \right) \theta + \frac{m_p z_{cg}}{I_y} \dot{u}_f - M_u u_f$$

$$- \left(M_{\dot w} + \frac{m_p x_{cg}}{I_y} \right) \dot{w}_f - M_w w_f = 0 \qquad (15)$$

This set of equations would apply for the three-degree-of-freedom tests if the k_{θ_m} terms were removed.

For the restricted degree of freedom tests, the following reduced sets of equations apply.

1. In two degrees of freedom, with $k_{\theta_m} = 0$:

θ, u_f ($w_f = 0$)

$$\dot{u}_f - \frac{m}{m_t} X_u u_f + \frac{m}{m_t} (g - X_w U_{o_f}) \theta = 0$$

$$\ddot{\theta} - (M_{\dot{\theta}} + M_w U_{o_f})\,\dot{\theta} - M_w U_{o_f}\,\theta + \frac{W_p\,z_{cg}}{I_y}\,\theta + \frac{m_p\,z_{cg}}{I_y}\,\dot{u}_f - M_u u_f = 0 \tag{16}$$

$\theta,\ w_f\ (u_f = 0)$

$$\dot{w}_f - Z_w w_f - Z_w U_{o_f}\,\theta = 0$$

$$\ddot{\theta} - (M_{\dot{\theta}} + M_w U_{o_f})\,\dot{\theta} - M_w U_{o_f}\,\theta$$
$$+ \frac{W_p\,z_{cg}}{I_y}\,\theta - \left(M_{\dot{w}} + \frac{m_p\,x_{cg}}{I_y}\right)\dot{w}_f - M_w w_f = 0 \tag{17}$$

2. In the single-degree-of-freedom experiments, with the mechanical spring and $u_f = 0$, $w_f = 0$, the equation that applies is

$$\ddot{\theta} - (M_{\dot{\theta}} + M_w U_{o_f})\,\dot{\theta} + \left(\frac{k_{\theta_m}}{I_y} - M_w U_{o_f} + \frac{W_p\,z_{cg}}{I_y}\right)\theta = 0 \tag{18}$$
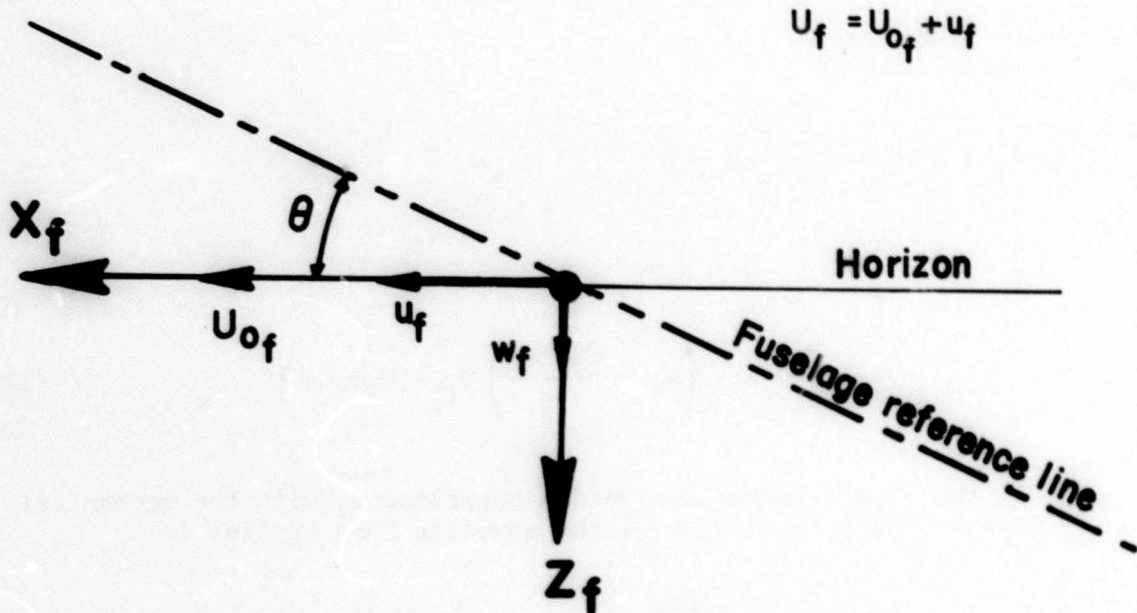
3. In the experiments where feedback is used, a term $M_{\Delta\beta_{PITCH}}\Delta\beta_{PITCH}$ should be added to the right-hand side of the pitching moment equation, and then the equation governing $\Delta\beta$ is

$$\Delta\beta_{PITCH} = K_{\dot{\theta}}\,\dot{\theta} \tag{19}$$
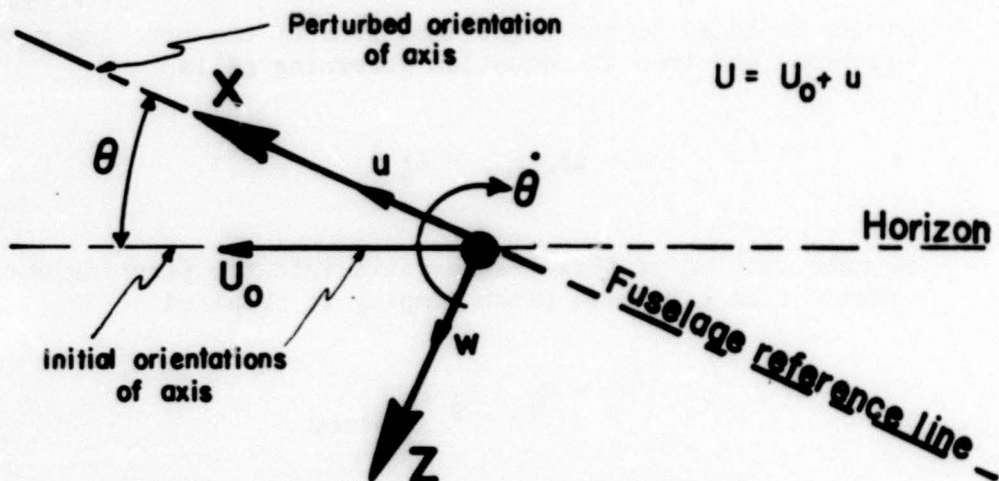
By substitution of these expressions into the pitching moment equation, an effective pitch damping is obtained

$$\bar{M}_{\dot{\theta}} = M_{\dot{\theta}} + K_{\dot{\theta}}\,M_{\Delta\beta_{PITCH}} \tag{20}$$

SPACE—FIXED AXIS

$$U_f = U_{o_f} + u_f$$

STABILITY AXIS

$$U = U_o + u$$

Perturbed orientation of axis
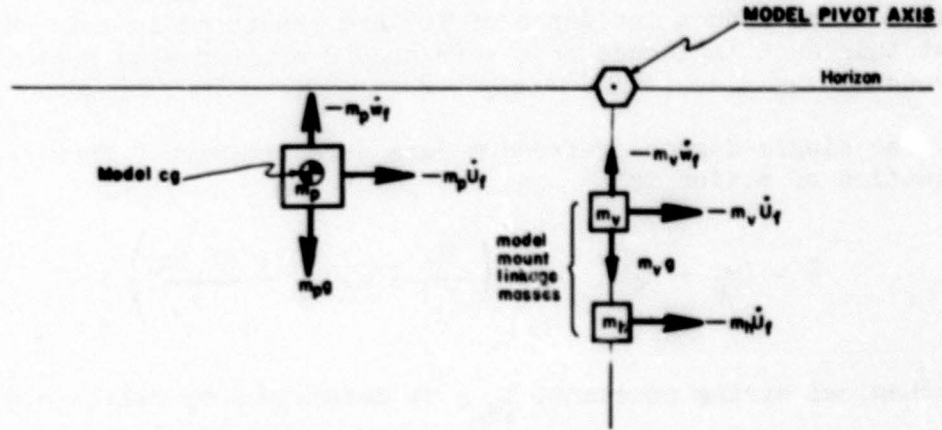
initial orientations of axis

(body fixed; initially aligned with freestream velocity at forward speeds or with horizon in hover)

Figure 15. Definitions of Space-Fixed and Stability Axis Systems (Variables Are Shown in Their Positive Sense).

MODEL AND LINKAGE MASS ARRANGEMENT

Note:

Lifted mass: $m = m_p + m_v$

Total horizontal mass: $m_t = m_p + m_v + m_h = m + m_h$

Mass ratio: $\dfrac{m}{m_t} = \dfrac{m_p + m_v}{m + m_h}$

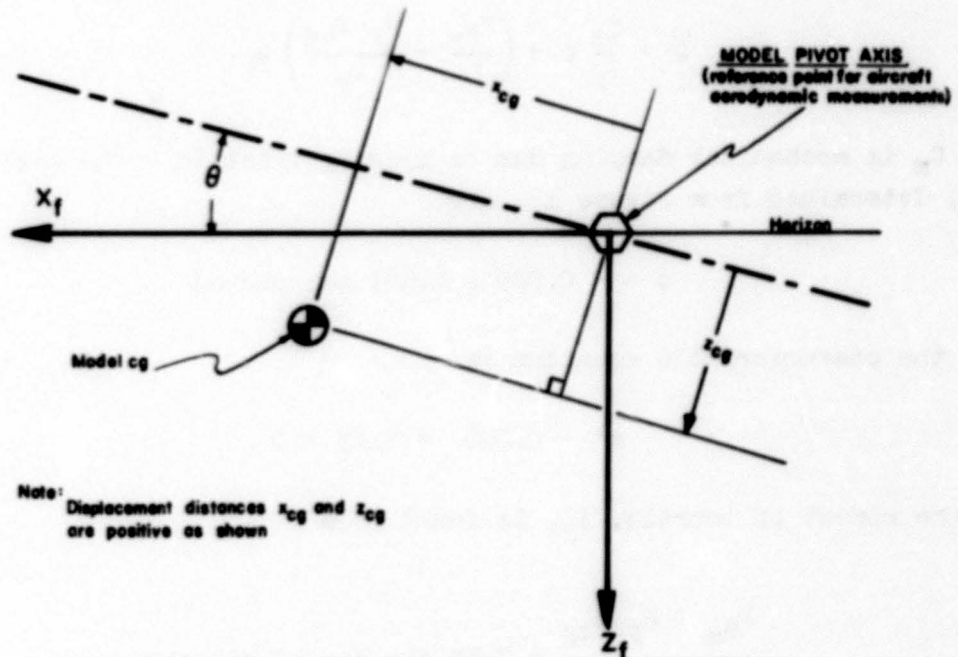
MODEL cg – PIVOT AXIS REFERENCE SYSTEM

Note: Displacement distances x_{cg} and z_{cg} are positive as shown

Figure 16. Model and Link Mass Arrangement and Reference System for Model cg and Pivot Axis.

53

UsedAPPENDIX II
NUMERICAL EXAMPLE

In order to illustrate in detail the method used to analyze the data, the calculations at a duct incidence of 70° are presented in this appendix. Data at this duct incidence from Reference 2 are repeated here in Figures 17 through 28.

First, the single-degree-of-freedom data were analyzed. From Appendix I, the equation of motion is

$$\ddot{\theta} - (M_{\dot{\theta}} + M_{\dot{w}}U_{o_f})\,\dot{\theta} + \left(\frac{k_{\theta_m}}{I_y} - M_w U_{o_f} + \frac{W_p\,z_{cg}}{I_y}\right)\theta = 0 \qquad (21)$$

The mechanical spring constant, k_{θ_m}, is determined by calibration to be 18.1 foot-pounds per radian; $W_p\,z_{cg}$ is found to be 1.89 foot-pounds per radian and arises from the fact that the cg of the model is below the pitching axis for this single-degree-of-freedom test. With the model's motor off and the forward velocity equal to zero, measurements were made to determine the moment of inertia. The aerodynamic damping is assumed to be negligible, and the equation of motion in this case is

$$\ddot{\theta} + \frac{C_m}{I_y}\,\dot{\theta} + \left(\frac{k_{\theta_m}}{I_y} + \frac{W_p\,z_{cg}}{I_y}\right)\theta = 0 \qquad (22)$$

where C_m is mechanical damping due to bearing friction. The measured roots, determined from Figure 17, are

$$s = -\,0.029 \pm 2.68i \text{ per second}$$

Thus, the characteristic equation is

$$s^2 + 0.058s + 7.15 = 0 \qquad (23)$$

Then the moment of inertia, I_y, is found from

$$\frac{k_{\theta_m} + W_p\,z_{cg}}{I_y} = 7.15 \text{ per second squared}$$

54

and is therefore equal to 2.80 slug-feet squared, and the mechanical damping, C_m/I_y, is equal to 0.058 per second. Balance weights present in the model-motor-off tests produced a moment of inertia increment of 0.65 slug-feet squared. The moment of inertia of the model for the tests at forward speed, with propellers running, is therefore 2.15 slug-feet squared.

At the trim speed for duct incidence equal to 70° (22 feet per second) and rpm equal to 6780, the single-degree-of-freedom roots measured from Figure 17 are

$$s = - 0.57 \pm 1.57i \text{ per second}$$

The characteristic equation is

$$s^2 + 1.14s + 2.785 = 0 \tag{24}$$

Thus, by comparison with equation (18),

$$\frac{W_p z_{cg}}{I_y} + \frac{k_{\theta_m}}{I_y} - M_w U_{o_f} = 2.785 \text{ per second squared}$$

$$- \left(\frac{C_m}{I_y} + M_{\dot{\theta}} + M_{\dot{w}} U_{o_f}\right) = 1.14 \text{ per second}$$

Substituting for W_p, z_{cg}, k_{θ_m}, I_y, and C_m,

$$M_w U_{o_f} = 6.62 \text{ per second squared}$$

$$- (M_{\dot{\theta}} + M_{\dot{w}} U_{o_f}) = 1.07 \text{ per second}$$

In all trim conditions, as in this example case, the mechanical damping was small in comparison to the aerodynamic damping.

The pendulous and mechanical spring terms are now removed from the equation of motion in order to proceed to the two-degree-of-freedom case. The resulting single-degree-of-freedom equation is

$$s^2 + 1.14s - 6.62 = 0 \tag{25}$$

The moment of inertia in the two- and three-degree-of-freedom cases was slightly different from the single-degree-of-freedom case due to balance

weights and is equal to 2.23 slug-feet squared. With this modification, the above equation becomes

$$s^2 + 1.09s - 6.39 = 0 \tag{26}$$

Now, in the two-degree-of-freedom case, the motion of the model was highly unstable, as shown in Figure 18, making it difficult to measure the period and damping when there was no feedback. The two-degree-of-freedom case with a feedback gain $K_{\dot{\theta}}$ equal to 0.044 second, shown in Figure 22, was analyzed, assuming that the damping increment produced by feedback (see Appendix I) was equal to that at the same feedback gain at a duct incidence of 80°. The increment at a duct incidence of 80° had been determined previously. From Appendix I, this damping increment $\Delta M_{\dot{\theta}}$ is equal to $K_{\dot{\theta}} M_{\Delta\beta_{PITCH}}$ and therefore is equivalent to assuming that the control effectiveness is the same at 80° as at 70°.

$\Delta M_{\dot{\theta}}$ was determined to be equal to $- 8.15$ per second at 80° duct incidence.

This value of damping is added directly to equation (26) to yield

$$s^2 + 9.24s - 6.39 = 0 \tag{27}$$

The roots of this equation are

$$s_1 = - 9.89 \text{ per second}$$
$$s_2 = + 0.65 \text{ per second}$$

Now we proceed to analyze the two-degree-of-freedom motion. Note that at this duct incidence the model cg was coincident with the pivot axis.

The equations of motion are, from Appendix I, (with x_{cg} and z_{cg} equal to zero),

$$\dot{u}_f - \frac{m}{m_t} X_u u_f + \frac{m}{m_t} (g - X_w U_{o_f}) \theta = 0$$

$$- M_u u_f + \ddot{\theta} - (\bar{M}_{\dot{\theta}} + M_{\dot{w}} U_{o_f}) \dot{\theta} - M_w U_{o_f} \theta = 0 \tag{28}$$

The notation $\bar{M}_{\dot{\theta}}$ implies that the damping includes the effect of feedback. m/m_t is the factor due to the model mounting linkage and is equal to 0.936.

Taking the Laplace transform of the above equations, and placing the characteristic equation in root locus form, considering M_u as the unknown parameter, we obtain

56

$$\frac{0.936\ M_u\ (g - X_w U_{o_f})}{(s - 0.936\ X_u)\left(s^2 - (\bar{M}_{\dot{\theta}} + M_{\dot{w}} U_{o_f})\ s - M_w U_{o_f}\right)} = -1 \qquad (29)$$

The quadratic factor in the denominator is that determined from the single-degree-of-freedom tests [equation (16)] and has roots equal to - 9.89 per second and + 0.65 per second.

Placing these known quantities in the above equation, we obtain

$$\frac{0.936\ M_u\ (g - X_w U_{o_f})}{(s - 0.936\ X_u)(s + 9.89)(s - 0.65)} = -1 \qquad (30)$$

The measured oscillatory dynamics for this two-degree-of-freedom case are (at $K_{\dot{\theta}} = 0.044$ second)

$$s = + 0.05 \pm 1.04i \text{ per second}$$

The known poles ($\triangle$) from the single-degree-of-freedom analysis and the experimentally measured roots ($\odot$) are shown on the complex plane in Figure 29.

Now, there is one unknown pole located at $0.936\ X_u$ ($\odot$). The location on the real axis is determined from the condition from equation (30): for positive M_u, the sum of the angle contributions from the poles ($\triangle$, $\odot$) at the roots ($\odot$) must be equal to $180°$. From Figure 29, the angle contributions from the two known poles are

$$s = + 0.65 \text{ per second} \qquad\qquad \alpha_1 = 117°$$
$$s = - 9.89 \text{ per second} \qquad\qquad \alpha_2 = 6°$$

The unknown pole ($0.936\ X_u$), therefore, must produce an angle contribution of $57°$ to make these three angles add up to $180°$. It is located at - 0.6 per second, as shown on Figure 29. This calculation yields a value of X_u equal to - 0.64 per second. Now the root locus for varying M_u is drawn as shown on Figure 29, and the gain at the experimental two-degree-of freedom roots ($\odot$) is calculated. This will determine the product $M_u\ (g - X_w U_{o_f})$. The gain calculation is

$$M_u\ (g - X_w U_{o_f}) = \frac{(1.17)(1.23)(10)}{0.936} = 15.40 \text{ per second cubed}$$

The isolated du· t data of Reference 1 indicate that $X_w U_{o_f}$ at this flight condition is negligible compared to g and, therefore,

$$M_u = 0.478 \text{ per foot-second}$$

With this information we can calculate the real root that corresponds to the two-degree-of-freedom motion from the characteristic equation. Taking the calculated values of M_u and X_u and placing them into equations (28), the characteristic equation is calculated

$$s^3 + 9.92 \, s^2 - 0.52s + 11.73 = 0 \tag{31}$$

The roots of equation (31) are

$$s_1 = -10.02 \text{ per second}$$
$$s_{2,3} = + \; 0.05 \pm 1.04i \text{ per second}$$

Now we return to the equations of motion (28) and rearrange the characteristic equation in root locus form, considering $M_{\dot{\theta}}$ as a variable parameter to determine the agreement among the derivatives found at a $K_{\dot{\theta}} = 0.44$ second and the other two-degree-of-freedom cases with different levels of rate feedback. In addition, the data can be extrapolated to calculate the dynamics of the vehicle with no feedback. The measured dynamics at other feedback gains from Figures 21 and 23 are

$$K_{\dot{\theta}} = 0.030 \text{ second} \qquad s = + \, 0.31 \pm 1.25i \text{ per second } (\text{⊙})$$

$$K_{\dot{\theta}} = 0.060 \text{ second} \qquad s = -\, 0.01 \pm 0.93i \text{ per second } (\text{⊚})$$

The equation for the root locus diagram for variable $M_{\dot{\theta}}$ is

$$\frac{(-\Delta M_{\dot{\theta}}) \, s(s - 0.936 \, X_u)}{(s - 0.936 \, X_u)\left(s^2 - (M_{\dot{\theta}} + M_w U_{o_f}) \, s - M_w U_{o_f}\right) + M_u (g - X_w U_{o_f})} = -1 \tag{32}$$

All of the stability derivatives in this expression have been determined except $\Delta M_{\dot{\theta}}$ and may be substituted giving

$$\frac{(-\Delta M_{\dot{\theta}}) \, s(s + 0.60)}{(s + 10.02)(s - 0.05 + 1.04i)(s - 0.05 - 1.04i)} = -1 \tag{33}$$

58

The root locus for variable $\Delta M_{\dot\theta}$ may now be sketched as shown in Figure 29. Note that this locus provides a verification of the previously calculated value of X_u, since it must pass through the other experimental points for different feedback gains. The $0°$ locus (---) shows the trend for decreasing feedback gain, and the $180°$ locus (——) shows the trend for increasing feedback gain. The root locus passes through the other two experimentally measured characteristic roots ($\odot$ $\odot$) and verifies the value of X_u. Now, the increment in damping provided at the experimental points, as well as the root location with no feedback, may be calculated.

The damping increments as calculated from the locus are

$$\text{From } K_{\dot\theta} = 0.044 \text{ second to } K_{\dot\theta} = 0.030 \text{ second}$$

$$\Delta M_{\dot\theta} = + 4.1 \text{ per second}$$

$$\text{From } K_{\dot\theta} = 0.044 \text{ second to } K_{\dot\theta} = 0.060 \text{ second}$$

$$\Delta M_{\dot\theta} = - 2.3 \text{ per second}$$

Now the location of the unaugmented roots of the vehicle may be calculated by finding the root location where $\Delta M_{\dot\theta} = + 8.15$ per second. This calculation yields for the characteristic roots of the unaugmented motion ($\odot$)

$$s = 1.00 \pm 1.45i \text{ per second}$$

The transient motion corresponding to this calculated result agrees closely with the time history of the measured model motion shown in Figure 18. The θ-w_f motion is shown in Figure 24. This motion was not analyzed due to the highly unstable character of the motion.

Now we proceed to consider the three-degree-of-freedom motion, using the data with feedback shown in Figure 28. Data at other levels of feedback are shown in Figures 26 and 27. It is assumed, as indicated by the static isolated duct data of Reference 1, that X_w is negligible. In this case, the complete characteristic equations (as obtained from equations (15), where $X_w = 0$, $z_{cg} = 0$, $x_{cg} = 0$, and $k_{\theta_m} = 0$) are

$$\dot{u}_f - \frac{m}{m_t} X_u u_f + \frac{m}{m_t} g\, \theta = 0$$

$$- Z_u u_f + \dot{w}_f - Z_w w_f - Z_w U_{o_f}\, \theta = 0$$

$$- M_u u_f - M_{\dot w}\dot{w}_f - M_w w_f + \ddot\theta - (M_{\dot\theta} + M_{\dot w}U_{o_f})\dot\theta - M_w U_{o_f}\, \theta = 0 \qquad (34)$$

59

The characteristic equation can be arranged in the following form:

$$s(\Delta_{\theta,u}) - Z_w \left((\Delta_{\theta,u})_0 - M_w \frac{Z_u g}{Z_w} \right) = 0 \qquad (35)$$

where $\Delta_{\theta,u}$ is the characteristic equation for the two-degree-of-freedom motion, and $(\Delta_{\theta,u})_0$ is the characteristic equation of the two-degree-of-freedom motion with $M_w = 0$. The coefficients of these two polynomials may be calculated. M_w is known from the one-degree-of-freedom analysis, and so we may find the two unknowns Z_u and Z_w as follows by placing this equation in root locus form, considering Z_u and Z_w as unknown.

$$\frac{- Z_w \left((\Delta_{\theta,u})_0 - M_w \frac{Z_u g}{Z_w} \right)}{s(\Delta_{\theta,u})} = -1 \qquad (36)$$

The poles of this expression are known, having been determined from the two-degree-of-freedom analysis. Note that this case has a feedback gain

$$K_{\dot{\theta}} = 0.030 \text{ second}$$

Thus, the characteristic equation that determines the poles is

$$\Delta_{\theta,u} = (s - 0.936 \, X_u)(s^2 - (\bar{M}_{\dot{\theta}} + M_w U_{O_f}) s - M_w U_{O_f}) + 0.936 \, g \, M_u \qquad (37)$$

Substituting the previously obtained values of the derivatives, this expression reduces to

$$\Delta_{\theta,u} = s^3 + 5.67 \, s^2 - 2.91 \, s + 11.83 \qquad (38)$$

The roots of this polynomial are

$$s_1 = -6.29 \text{ per second}$$
$$s_{2,3} = +0.31 \pm 1.25i \text{ per second}$$

and are the poles, along with $s = 0$, of the root locus expression, equation (36), and are shown on Figure 29 (⊙).

60

Part of the numerator of equation (36) is calculated with $M_w = 0$ and is equal to

$$(\Delta_{\theta,u})_o = s^3 + 5.67 \, s^2 + 3.04 + 15.4$$

The roots of this polynomial are

$$s_1 \quad = -5.18 \text{ per second}$$
$$s_{2,3} = -0.065 \pm 1.73i \text{ per second}$$

and are also shown on Figure 29 ($\odot$).

First we sketch the root locus for the factor in brackets in the numerator, expressing it in root locus form as

$$\frac{-M_w \dfrac{Z_u g}{Z_w}}{(\Delta_{\theta,u})_o} = -1 \tag{39}$$

Now, this root locus is drawn on Figure 29 (---), and the location of roots (taken in conjunction with the complete root locus equation), that satisfies the 180°-angle condition at the three-degree-of-freedom experimental roots ($\boxdot$) is determined. The experimentally determined characteristic roots for the three-degree-of-freedom motion are,

$$s_{1,2} = +0.25 \pm 1.32i \text{ per second}$$

The location of the roots of equation (39), which are the zeros of the root locus equation (36), was found to be at

$$s_1 \quad = -4.56 \text{ per second}$$
$$s_{2,3} \quad = -0.32 \pm 0.76i \text{ per second}$$

and are shown on Figure 29 as ($\ominus$).

Then the gain at this point is calculated to yield the value

$$M_w \frac{Z_u g}{Z_w} = 13.1 \text{ per second cubed} \tag{40}$$

Now we may sketch the complete root locus based on equation (36) to determine Z_w with poles ($\odot$) and zeros ($\ominus$). The locus is drawn with Z_w varying and the ratio Z_u/Z_w constant as shown on Figure 29 (—).

The gain calculation yields

$$Z_w = -0.137 \text{ per second}$$

Then, knowing M_w, the value of Z_u is calculated from equation (40) as

$$Z_u = -0.19 \text{ per second}$$

This completes the analysis of the 70° case and this numerical example.

The analysis of the other cases follows a similar procedure as described in the text.
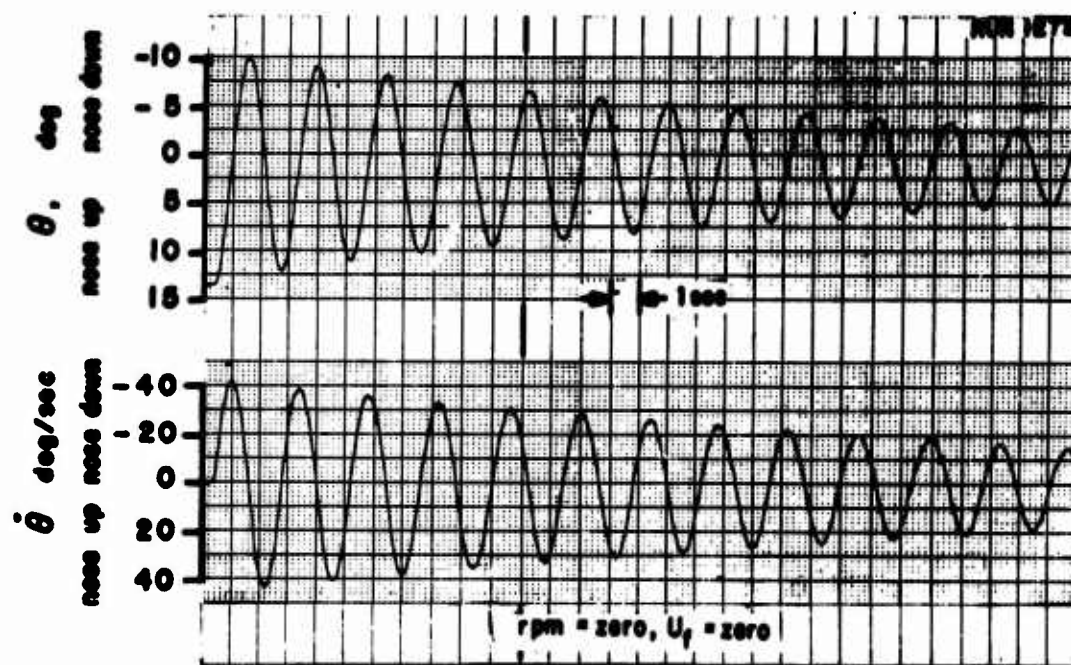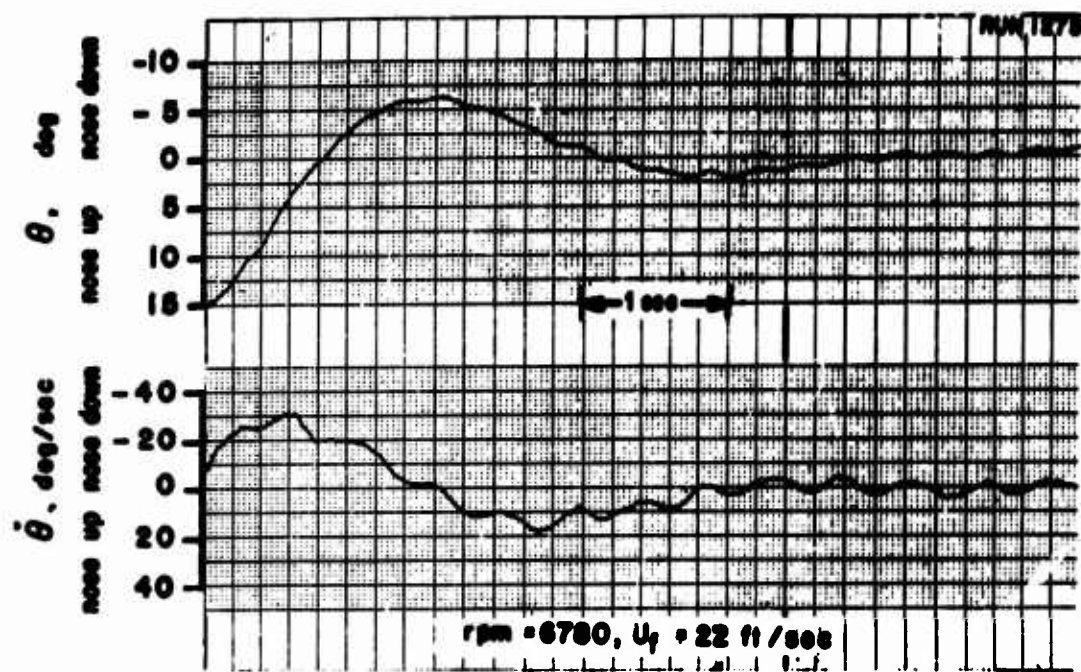
Figure 17. Self-Excited Transient Response. One Degree of Freedom, θ.
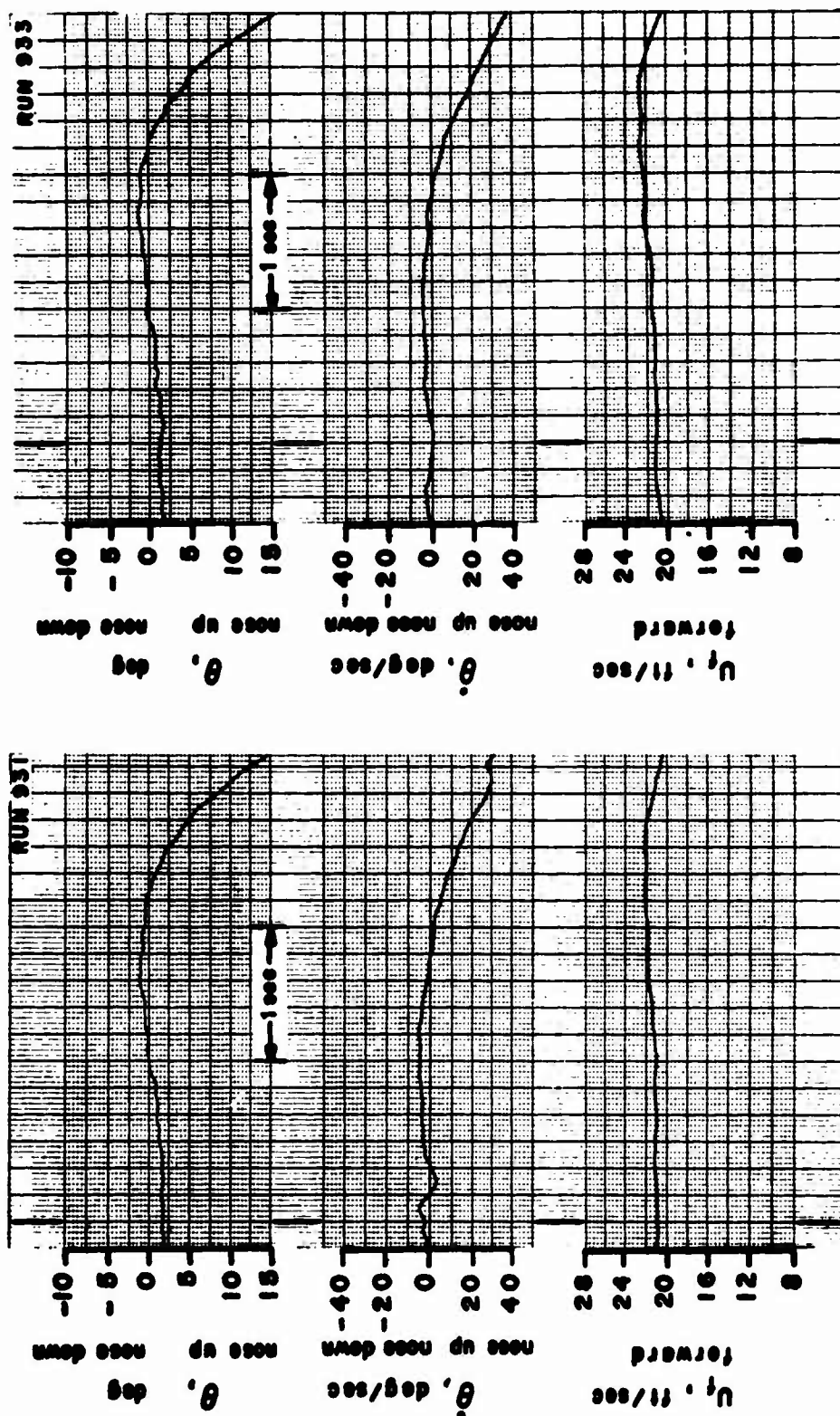No Stability Augmentation. i_d = 70°, $\beta_{.75R}$ = 25.2°.

Figure 18. Self-Excited Transient Responses. Two Degrees of Freedom, $\theta-U_f$. No Stability Augmentation. $i_d = 70°$, $\beta_{.75R} = 26.2°$, rpm = 6780.
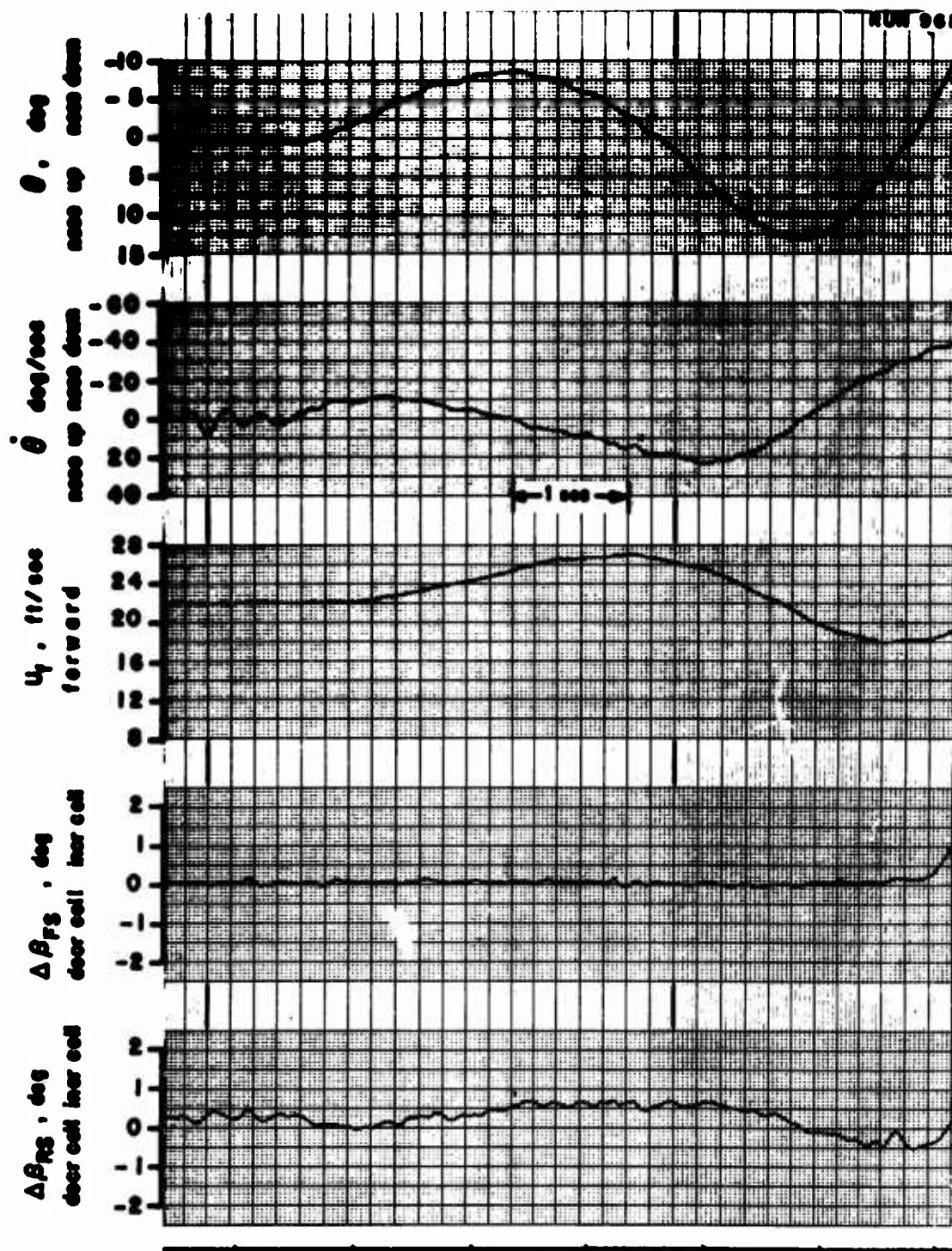
64
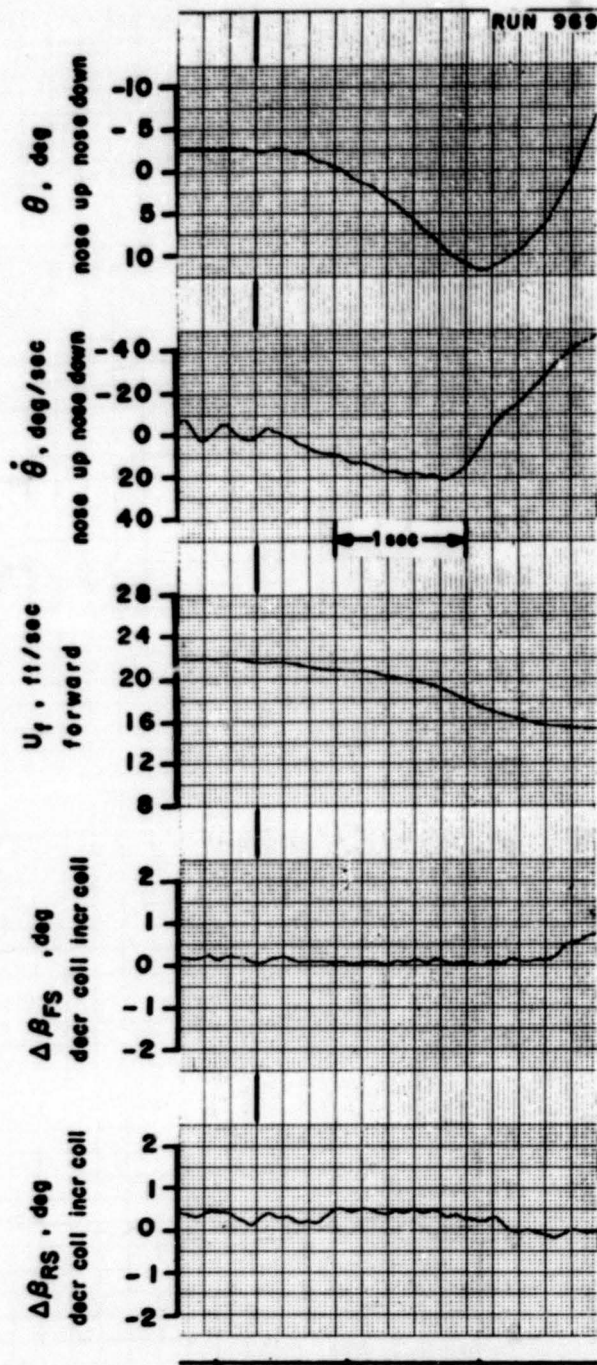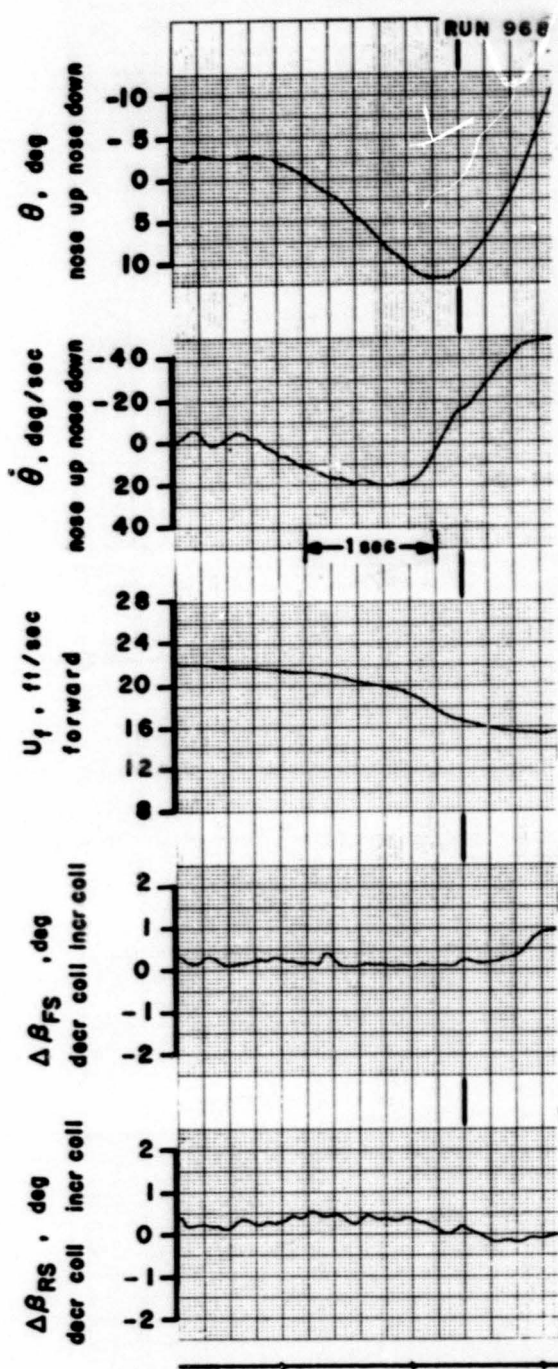
Figure 19.   Self-Excited Transient Responses.   Two Degrees of Freedom, θ-U_f. $K_{\dot{\theta}}$ = 0.021 sec. i_d = 70°, $\beta_{.75R}$ = 26.2°, rpm = 6780.

Figure 20. Self-Excited Transient Responses. Two Degrees of Freedom, θ-U_f. $K_{\dot{\theta}}$ = 0.027 sec. i_d = 70°, $\beta_{.75R}$ = 26.2°, rpm = 6780.
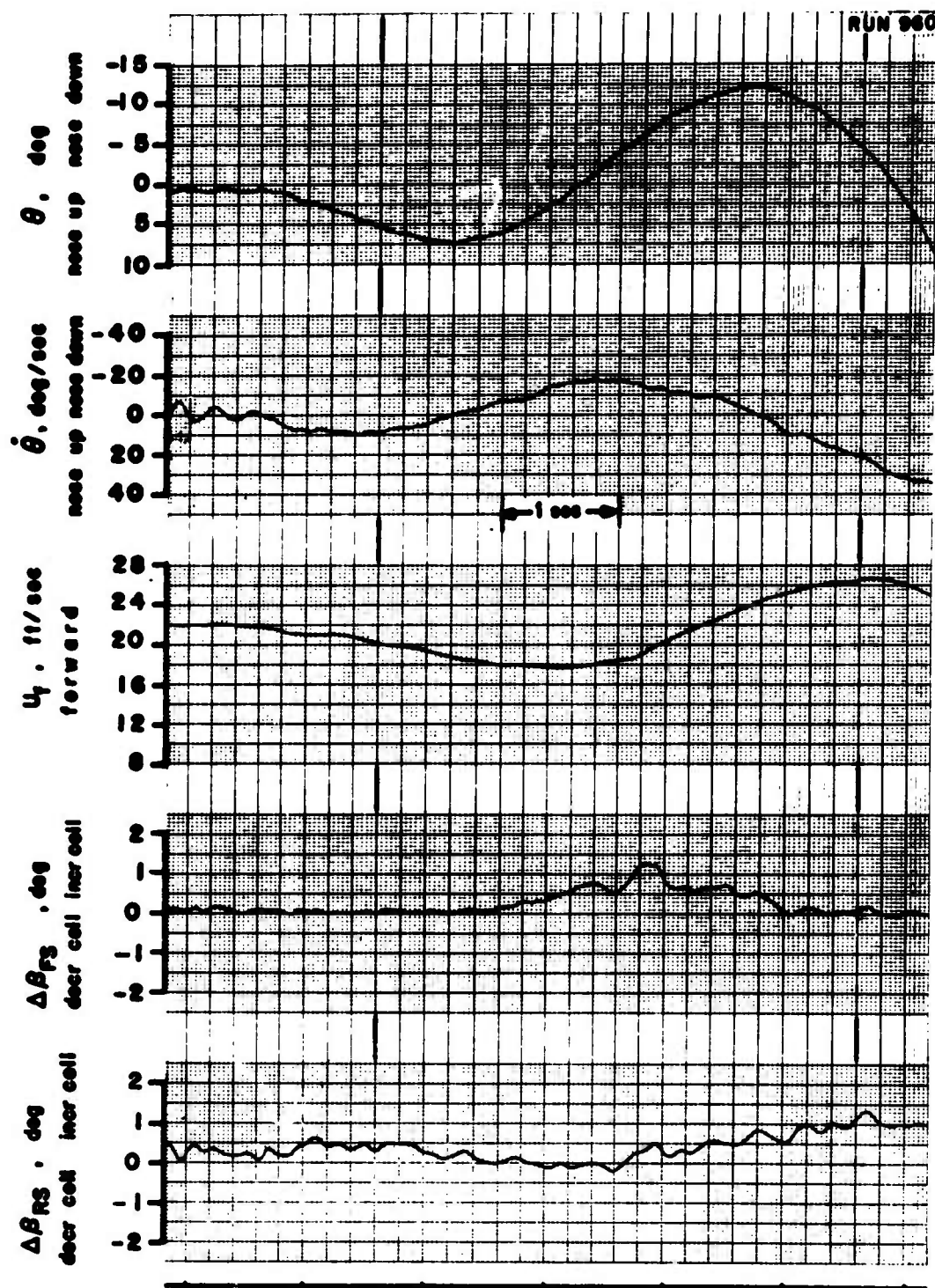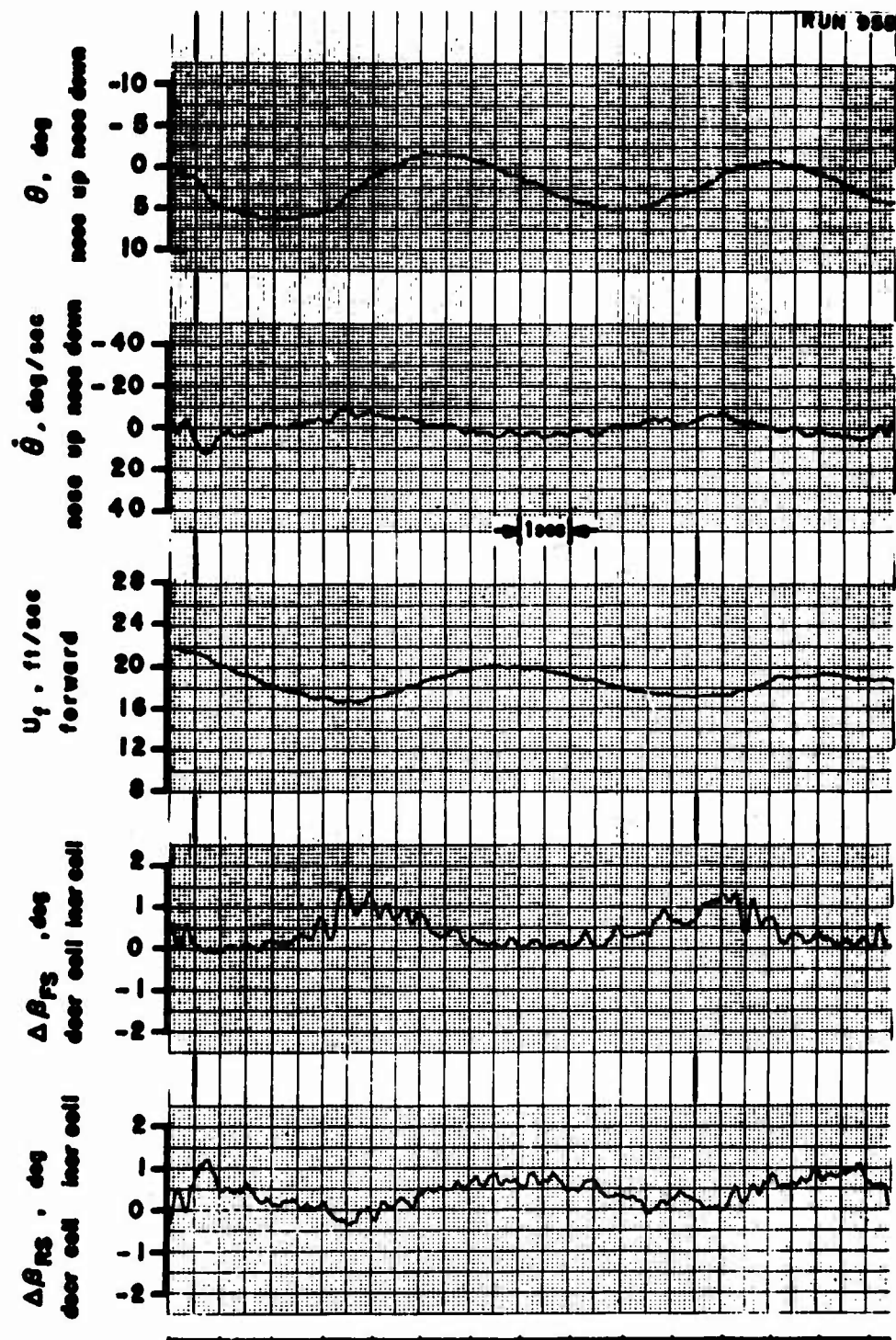
Figure 21. Self-Excited Transient Responses. Two Degrees of Freedom, $\theta - U_f$. $K_{\dot{\theta}}$ = 0.030 sec. i_d = 70°, $\beta_{.75R}$ = 26.2°, rpm = 6780.

Figure 22. Self-Excited Transient Responses. Two Degrees of Freedom, $\theta - U_f$. $K_{\dot{\theta}} = 0.044$ sec. $i_d = 70°$, $\beta_{.75R} = 26.2°$, rpm = 6780.

68

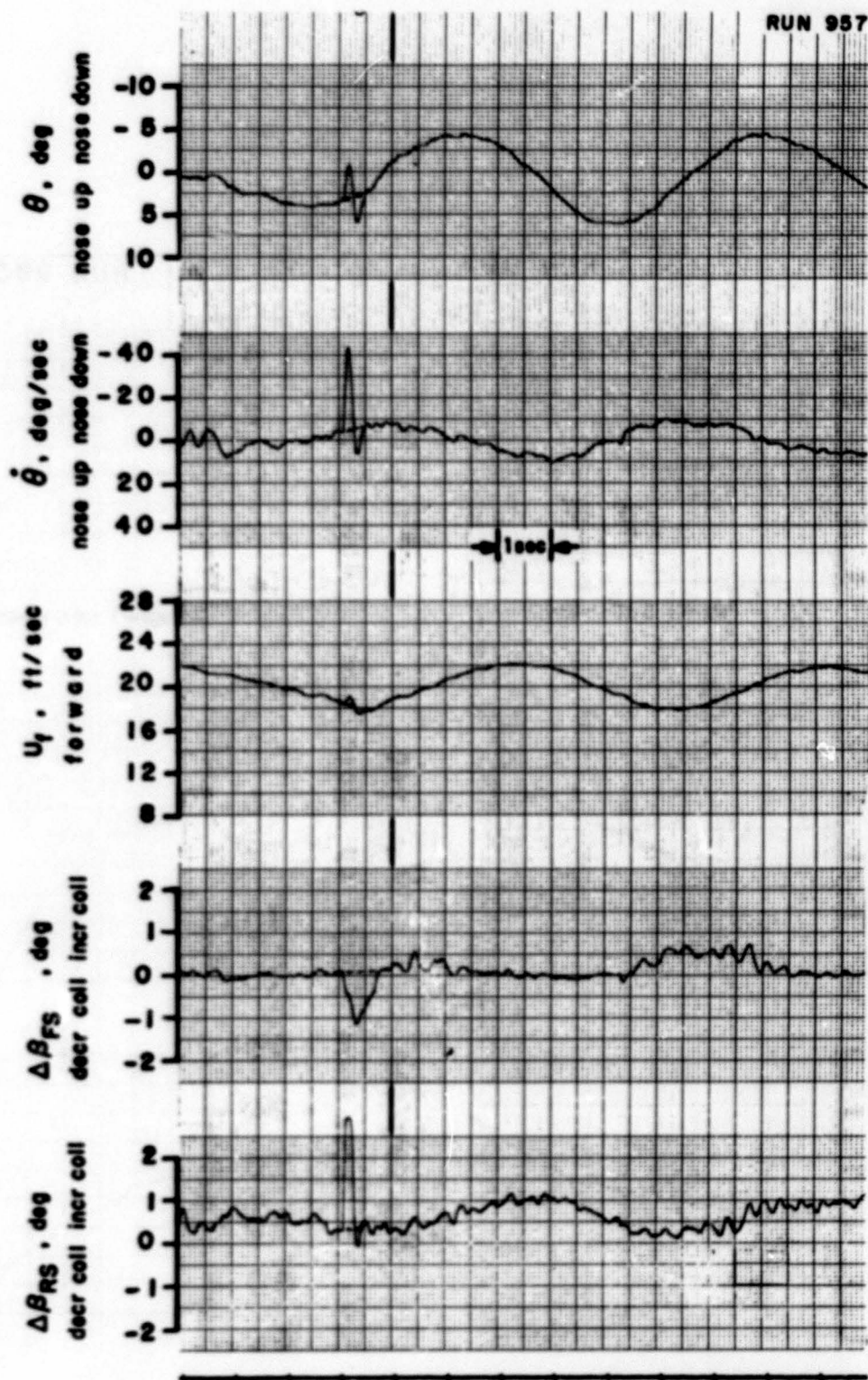Figure 23. Self-Excited Transient Responses. Two Degrees of Freedom, θ-U_f. $K_\theta = 0.060$ sec. $i_d = 70°$, $\beta_{.75R} = 26.2°$, rpm = 6780.
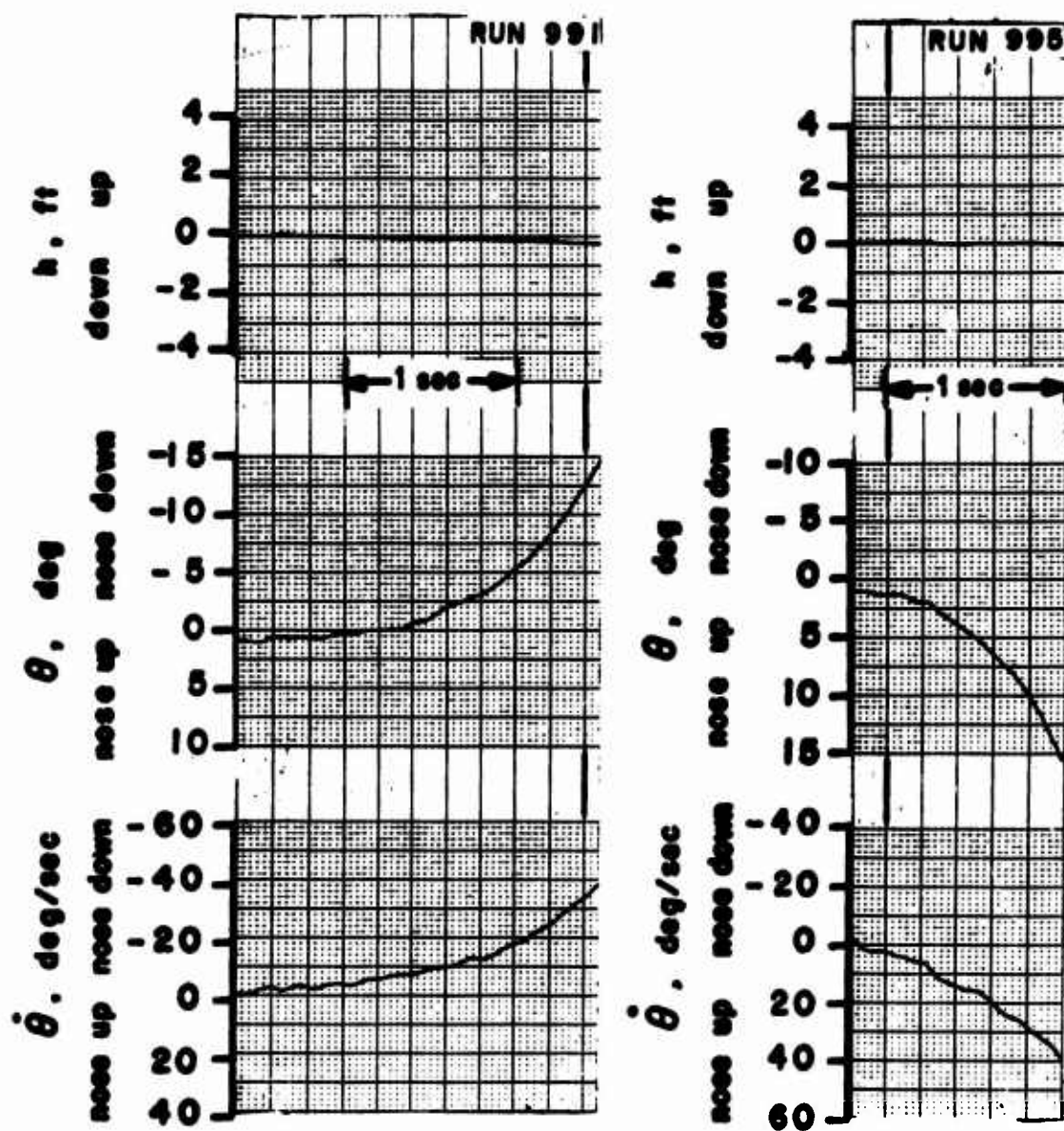
Figure 24. Self-Excited Transient Responses. Two Degrees of Freedom, θ-w_f. No Stability Augmentation. $i_d = 70°$, $\beta_{.75R} = 26.2°$, rpm = 6780.
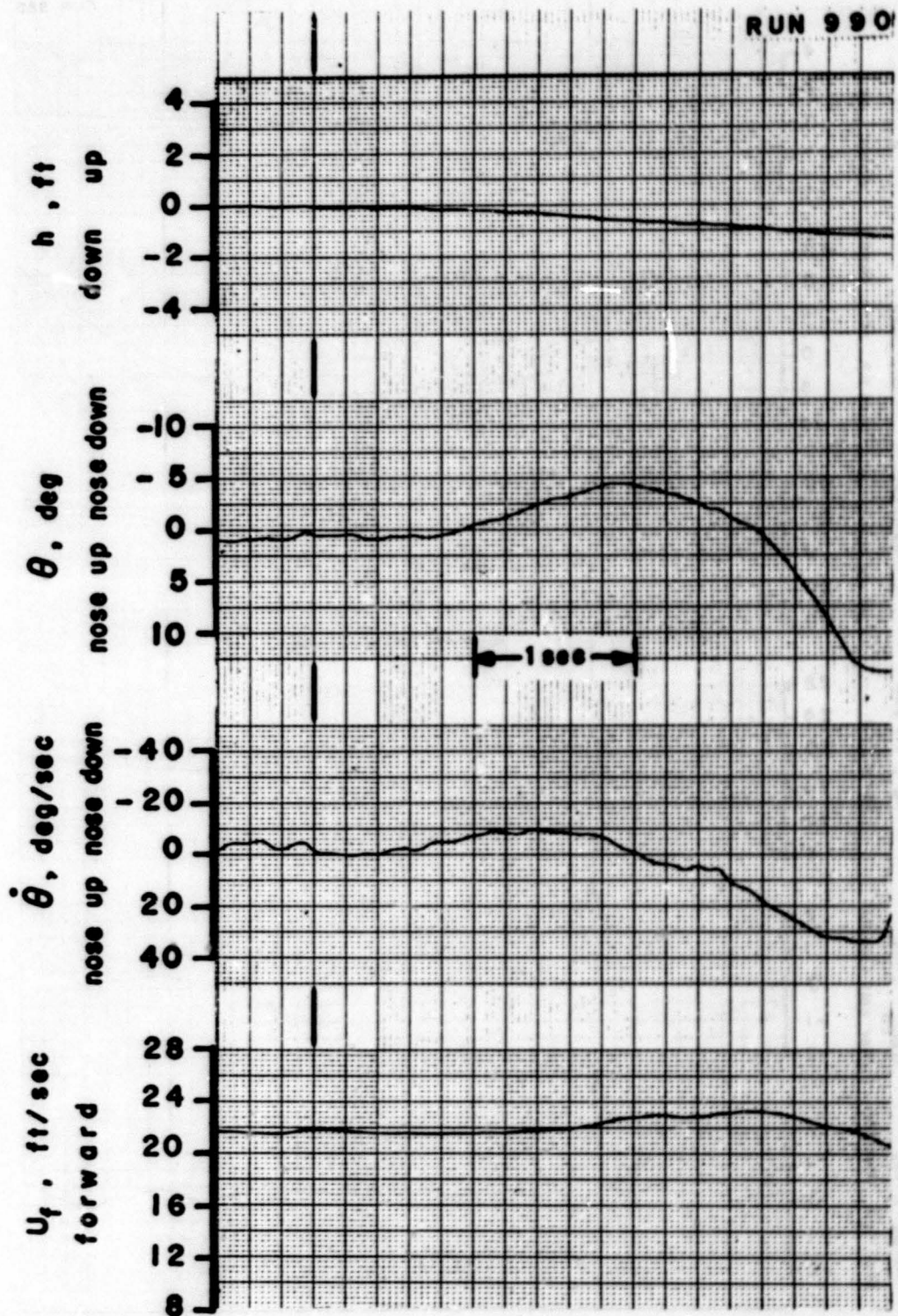
Figure 25. Self-Excited Transient Responses. Three Degrees of Freedom, θ-U_f-w_f. No Stability Augmentation. i_d = 70°, $\beta_{.75R}$ = 26.2°, rpm = 6780.
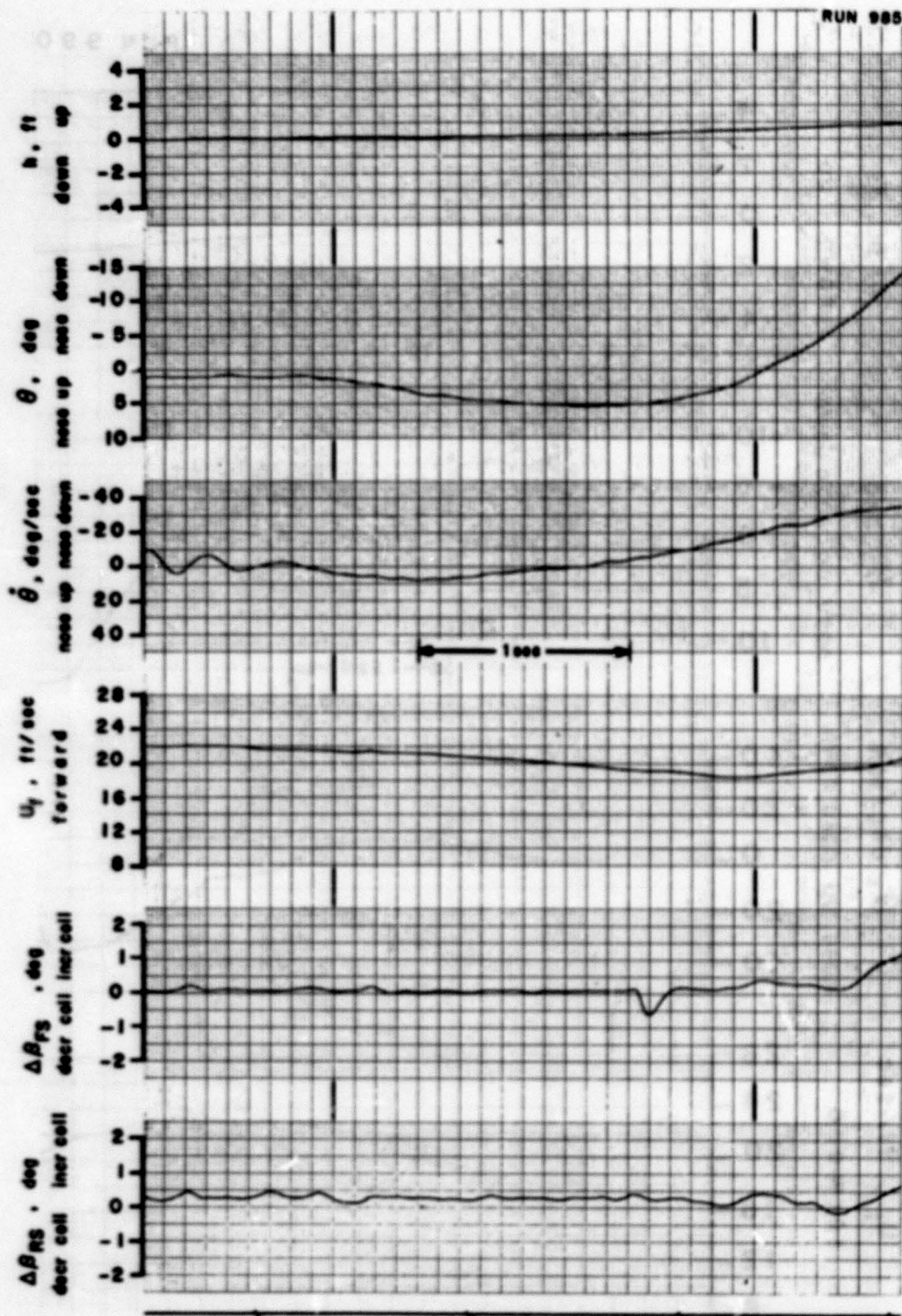
Figure 26.   Self-Excited Transient Responses.   Three Degrees of Freedom,
θ-U_f-w_f. $K_{\dot{\theta}}$ = 0.021 sec. i_d = 70°, $\beta_{.75R}$ = 26.2°, rpm = 6780.

72

Figure 27. Self-Excited Transient Responses. Three Degrees of Freedom, $\theta-U_f-w_f$. $K_\theta = 0.027$ sec. $i_d = 70°$, $\beta_{.75R} = 26.2°$, rpm = 6780.
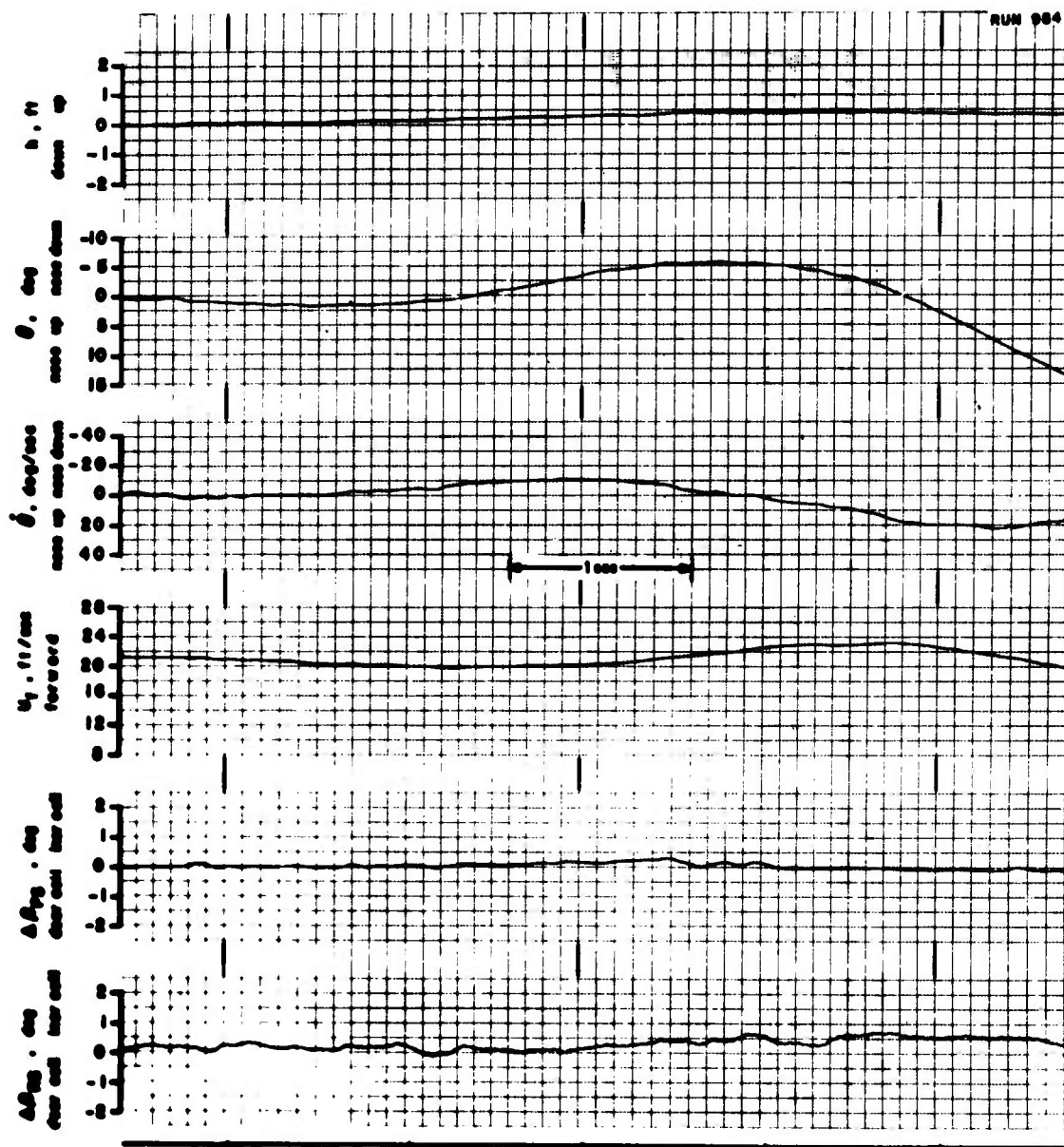
73
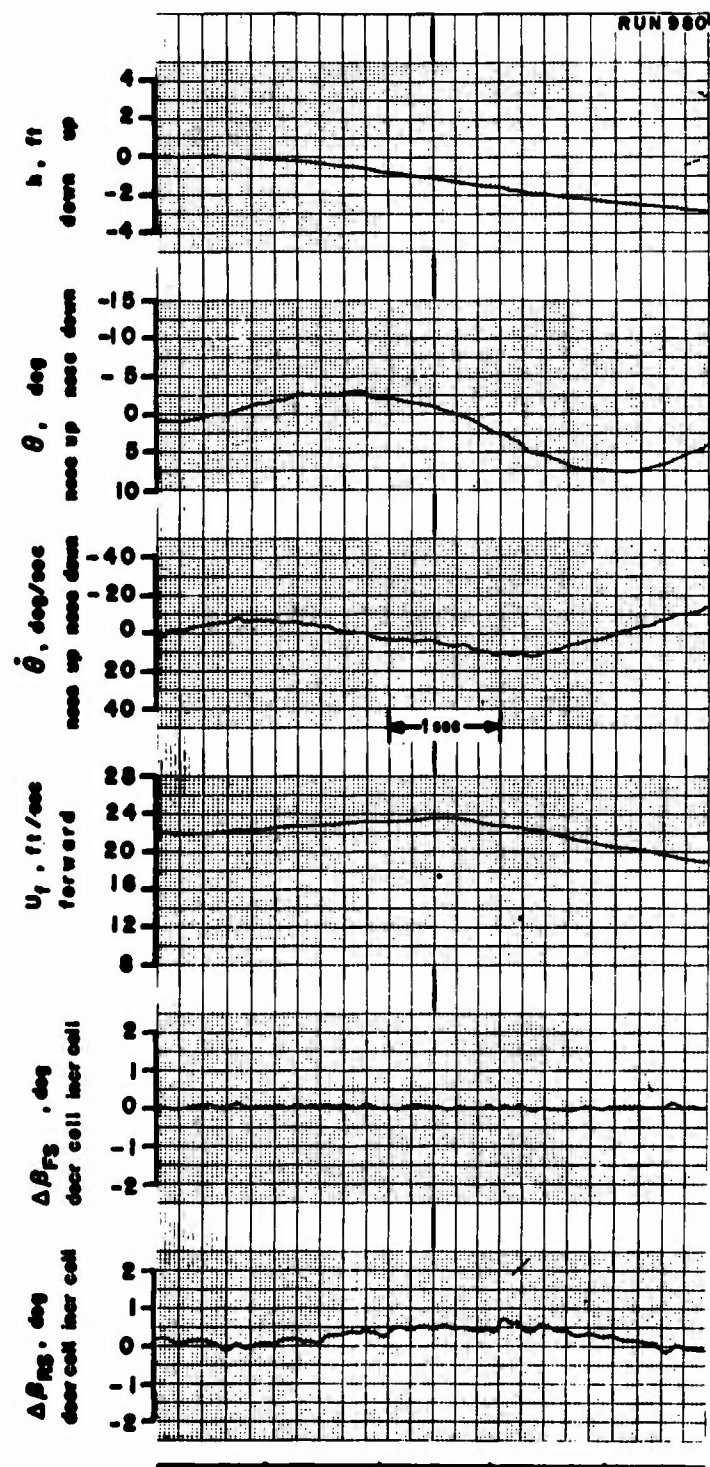
Figure 28. Self-Excited Transient Responses. Three Degrees of Freedom,
θ-U_f-w_f. $K_{\dot\theta}$ = 0.030 sec. i_d = 70°, $\beta_{.75R}$ = 26.2°, rpm = 6780.

74

DEGREES OF FREEDOM

△ ONE DEGREE OF FREEDOM, θ (data)
⊙⊙ TWO DEGREES OF FREEDOM, $\theta - u_f$ (data)
⬡ POLE (calculated)

NOTE: PITCH RATE FEEDBACK $K_{\dot\theta} = 0.044$ sec

Figure 29. Root Locus Diagram for Analysis of 70° Duct Incidence Data.

75

Figure 29. Continued

Figure 29. Concluded

77

APPENDIX III
CONVERSION TO FULL SCALE

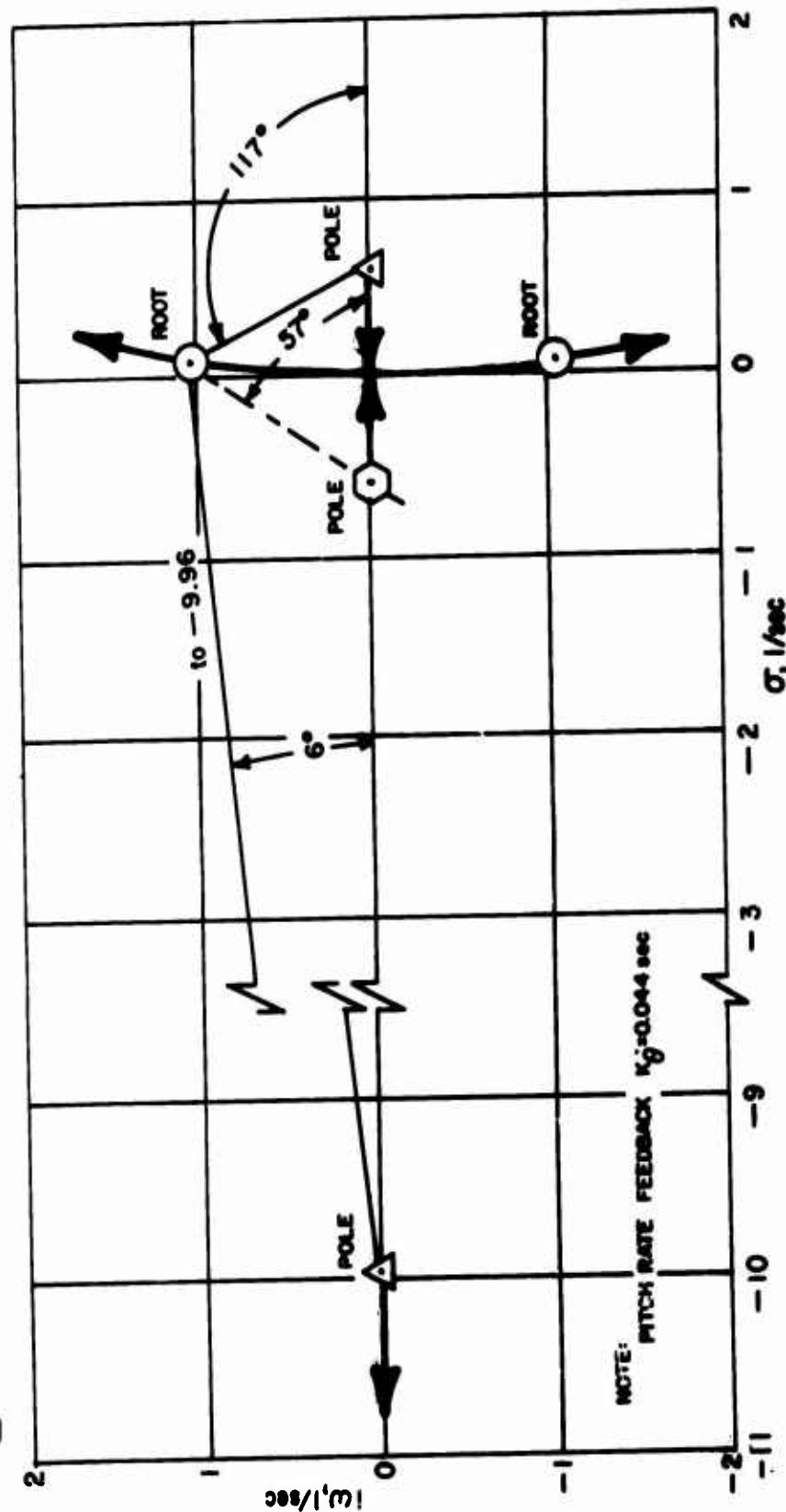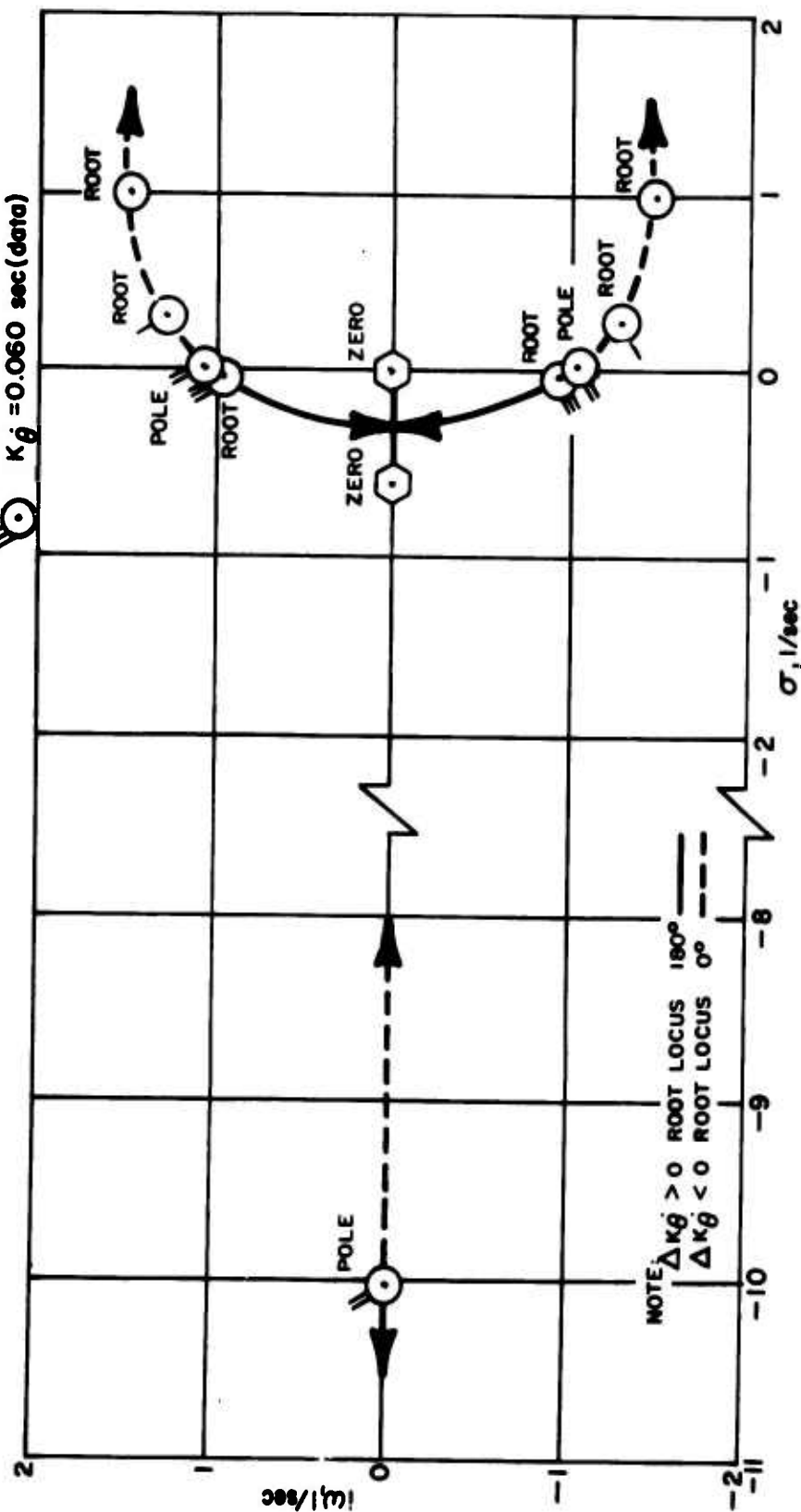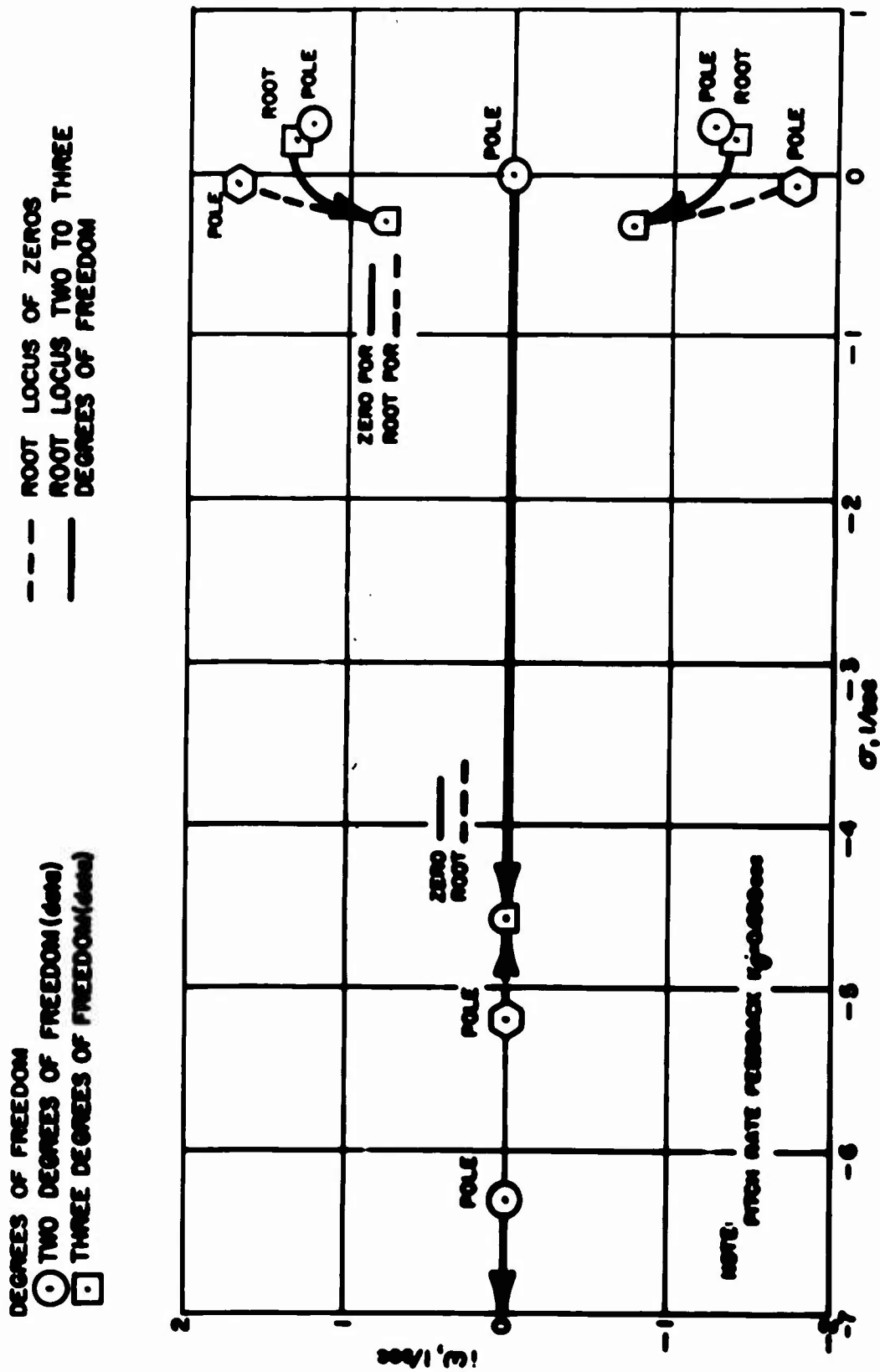The results of the model experiments may be converted to correspo. 1 to a
variety of full-scale vehicles of similar geometry to the model. It is
convenient to consider the scaling of the data in two steps.

First, the size of the model is accounted for by using the dynamic model
scale factors given in Table II. The full-scale aircraft of interest here
has a linear scale factor of 0.145; however, other scale factors may be
selected to correspond to other geometrically similar aircraft of desired
size. This scaling will imply a certain gross weight for the full-scale
vehicle.

Second, the results may be interpreted at other gross weights by varying
certain of the parameters involved, maintaining the lift coefficient (or
equivalently, the propeller thrust coefficient based on forward speed)
constant. As the gross weight is varied, either the forward speed or the
ambient air density can be varied to preserve the equilibrium lift
coefficient.

These two interpretations, and the appropriate factors to use for gross
weight variation, are given in Table V. We consider here only the effects
of changes in gross weight; the size considerations have been taken into
account.

VELOCITY - GROSS WEIGHT CORRESPONDENCE

Maintaining the equilibrium lift coefficient of the vehicle at two differ-
ent gross weights, at the same altitude, yields the following relationship
between flight velocity and gross weight:

$$\frac{W_t}{V_t^2} = \frac{W_0}{V_0^2}$$

Defining a weight ratio scale factor as

$$\Lambda = \frac{W_0}{W_t}$$

the velocity is scaled as

$$\frac{V_0}{V_t} = \sqrt{\Lambda}$$

The advance ratio must also be maintained constant, and so this scaling results in a different rpm; i.e.,

$$\frac{\Omega_0}{\Omega_c} = \sqrt{\Lambda_w}$$

In the case of the experiments conducted, Ω_0 will not correspond to the full-scale rotational speed of the ducted propeller, since the model rpm was selected on the basis of a proper value of Ω_c. Scale factors for conversion of the data in this fashion are given in Table V.

It is possible to make an assumption that will make a wider interpretation of the data possible. This assumption is similar to the use of the propeller thrust coefficient to characterize data on tilt-wing aerodynamics. That is, if we assume that the aerodynamic stability characteristics of the vehicle depend primarily on the ratio of forward speed to duct exit velocity and not on the particular combination of blade angle and advance ratio used to produce this velocity, it may be assumed that blade angle and rpm are interchangeable and the scaled data may be applied to other rotational speeds.

The validity of this assumption has not been checked. Hovering flight data indicate that there are differences in the dynamics depending upon the combination of blade angle and rpm used to produce a given thrust, so this approximation should be applied with care if used at all.

AIR DENSITY - GROSS WEIGHT CORRESPONDENCE

Alternately, the lift coefficient may be maintained constant by varying ambient air density in proportion to gross weight:

$$\frac{W_c}{\rho_c} = \frac{W_0}{\rho_0}$$

Then the data may be interpreted on this basis, where the aerodynamic forces will vary by the scale factor Λ_w and the reduced gross weight will be equivalent to flight at a different altitude given by

$$\frac{\rho_0}{\rho_c} = \Lambda_w$$

In this case, note that

$$V_0 = V_c$$

The scale factors for conversion by this method are also given in Table V.

79

In this case, it may be observed that there will be no change in the dynamic stability characteristics of the aircraft. This result indicates that in many cases it is desirable, for comparison with flight test, to test a model that is overweight on the basis of the dynamic scaling law, since the flight test experiments will always be conducted at altitudes above sea level. This correspondence for the experiments conducted here is shown in Figure 14.

DISTRIBUTION

US Army Materiel Command	6
US Army Aviation Systems Command	6
United States Continental Army Command	1
United States Army, Pacific	1
Chief of R&D, DA	2
Director of Defense Research and Engineering	2
US Army R&D Group (Europe)	2
US Army Aviation Materiel Laboratories	23
US Army Limited War Laboratory	1
US Army Human Engineering Laboratories	2
Army Aeronautical Research Laboratory, Ames Research Center	1
US Army Research Office-Durham	1
US Army Test and Evaluation Command	1
US Army Electronics Command	2
US Army Combat Developments Command, Fort Belvoir	2
US Army Combat Developments Command Experimentation Command	1
US Army Combat Developments Command Transportation Agency	1
US Army Combat Developments Command Aviation Agency	1
US Army War College	1
US Army Command and General Staff College	1
US Army Aviation School	1
Deputy Chief of Staff for Personnel, DA	1
Assistant Chief of Staff for Force Development, DA	2
US Army Tank-Automotive Command	2
US Army Armor and Engineer Board	1
US Army Aviation Systems Test Activity, Edwards AFB	2
Air Force Flight Test Center, Edwards AFB	2
US Army Field Office, AFSC, Andrews AFB	1
Air Force Materials Laboratory, Wright-Patterson AFB	2
Air Force Flight Dynamics Laboratory, Wright-Patterson AFB	19
AMRL, Wright-Patterson AFB	1
Systems Engineering Group, AFSC, Wright-Patterson AFB	2
Naval Air Systems Command, DN	11
Naval Ship Engineering Center	1
Office of Naval Research	3
US Naval Research Laboratory	1
US Naval Air Test Center, Patuxent River	1
Naval Air Propulsion Test Center, Philadelphia	1
Naval Air Development Center, Johnsville	1
Helicopter Combat Support Squadron TWO, NAS, Lakehurst	1
Naval Weapons Laboratory, Dahlgren	1
Commandant of the Marine Corps	1
Marine Corps Liaison Officer, US Army Transportation School	1

DOCUMENT CONTROL DATA - R & D

(Security classification of title, body of abstract and indexing annotation must be entered when the overall report is classified)

1. ORIGINATING ACTIVITY (Corporate author)	2a. REPORT SECURITY CLASSIFICATION
Department of Aerospace and Mechanical Sciences	Unclassified
Princeton University	2b. GROUP
Princeton, New Jersey	-

3. REPORT TITLE

AN INVESTIGATION OF THE DYNAMIC STABILITY CHARACTERISTICS OF A QUAD CONFIGURATION, DUCTED-PROPELLER V/STOL MODEL, VOLUME IV - THE LONGITUDINAL STABILITY CHARACTERISTICS OF A QUAD CONFIGURATION, DUCTED-PROPELLER V/STOL MODEL AT HIGH DUCT INCIDENCE

4. DESCRIPTIVE NOTES (Type of report and inclusive dates)

Final Technical Report

5. AUTHOR(S) (First name, middle initial, last name)

Howard C. Curtiss, Jr.

6. REPORT DATE	7a. TOTAL NO. OF PAGES	7b. NO. OF REFS
May 1969	95	6

8a. CONTRACT OR GRANT NO.	9a. ORIGINATOR'S REPORT NUMBER(S)
DAAJ02-67-C-0025	
b. PROJECT NO.	USAAVLAB Technical Report 68-49D
Task 1F162204A14233	
c.	9b. OTHER REPORT NO(S) (Any other numbers that may be assigned this report)
d.	Aerospace Sciences Report 848

10. DISTRIBUTION STATEMENT

This document is subject to special export controls and each transmittal to foreign governments or foreign nationals may be made only with prior approval of US Army Aviation Materiel Laboratories, Fort Eustis, Virginia 23604.

11. SUPPLEMENTARY NOTES	12. SPONSORING MILITARY ACTIVITY
Volume IV of a 4-volume report.	U. S. Army Aviation Materiel Laboratories Fort Eustis, Virginia

13. ABSTRACT

The results of experiments conducted to determine the dynamic stability characteristics of a dynamically similar model of quad-duct V/STOL aircraft are reported in References 1 and 2. Portions of these data that pertain to the longitudinal dynamics of the vehicle at five duct incidences were analyzed to determine the stability derivatives of the vehicle. The analysis and the resulting stability derivatives are presented and discussed in this report.

The measured time histories indicated that the data could be analyzed on the basis of linearized small perturbation equations. Root locus techniques were used to analyze the data.

The full-scale derivatives determined from the analysis that correspond to a vehicle very similar to the Bell X-22A are presented.

The transient motions of the model were unstable at all duct incidences except $50°$, the lowest incidence investigated.

14. KEY WORDS	LINK A		LINK B		LINK C	
	ROLE	WT	ROLE	WT	ROLE	WT
V/STOL Dynamic Stability Analysis of Experimental Data Longitudinal Dynamics Bell X-22A						

5288-69